Universidade de Aveiro
2019

Departamento de Engenharia
de Materiais e Cerâmica

Diogo João Breda Lopes

Design de fotocatalisadores multifuncionais à base de titânia por reações redox controladas

Design of multifunctional titania-based photocatalysts by controlled redox reactions

2019

Universidade de Aveiro
2019

Departamento de Engenharia
de Materiais e Cerâmica

Diogo João Breda Lopes

Design de fotocatalisadores multifuncionais à base de titânia por reações redox controladas

Design of multifunctional titania-based photocatalysts by controlled redox reactions

Dissertação apresentada à Universidade de Aveiro para cumprimento dos requisitos necessários à obtenção do grau de Mestre em Engenharia de Materiais, realizada sob a orientação científica do Doutor Andrei Kavaleuski, Investigador Principal do Departamento de Engenharia de Materiais e Cerâmica da Universidade de Aveiro e co-orientação da Doutora Ana Luísa Daniel da Silva, Investigadora Auxiliar do Departamento de Química da Universidade de Aveiro.

o júri

presidente

Prof. Doutor João António Labrincha Batista
Professor Associado do Departamento de Engenharia de Materiais e Cerâmica da Universidade de
Aveiro

Doutor Aliaksandr Shaula
Investigador do Centro de Tecnologia Mecânica e Automação da Universidade de Aveiro

Doutor Andrei Kavaleuski
Investigador Principal do Departamento de Engenharia de Materiais e Cerâmica, CICECO da
Universidade de Aveiro

agradecimentos

O presente trabalho representa o culminar de mais uma fase na minha vida académica e gostava de agradecer a todos os que me acompanharam neste trajeto.

Ao Doutor Andrei Kavaleuski e à Doutora Ana Luísa Silva pela orientação, dedicação, ajuda e disponibilidade como orientadores deste trabalho.

Agradeço também a todas as pessoas dos Departamentos de Engenharia de Materiais e Cerâmica e Química que contribuíram para este trabalho ao disponibilizarem o seu tempo para me ajudar com a utilização de equipamento, análise de dados e partilha de conhecimento.

palavras-chave Fotocatálise; TiO_2; anatase; rutilo; planeamento de Taguchi; reações redox; óxido-carboneto de titânio; microstrutura core-shell.

resumo O presente trabalho teve como objetivo o design da composição de fases e microestrutura de compósitos à base de rutilo – carboneto de silício, através de reações redox controladas, visando a preparação de fotocatalizadores multifuncionais à base de titânia, com capacidades inerentes de coativação térmica e estabilização do polimorfo anatase. Os materiais foram processados utilizando um método convencional de processamento no estado sólido, envolvendo uma redução parcial do rutilo através do SiC numa atmosfera inerte de árgon, seguido por uma pós-oxidação em ar. O impacto das condições de processamento na composição de fases das amostras oxidadas e a sua atividade fotocatalítica foram avaliadas utilizando o método experimental de Taguchi. As análises de DRX confirmaram a presença de misturas rutilo/anatase nas amostras oxidadas. Os resultados enfatizam que as temperaturas de pré-redução e pós-oxidação são os parâmetros mais críticos na definição da composição de fases, enquanto que o tempo de pós-oxidação parece ser relevante para o desempenho fotocatalítico. Estudos microestruturais revelaram a formação de partículas core-shell nas amostras pré-reduzidas e pós-oxidadas, que podem suprimir a atividade fotocatalítica. A maior velocidade de reação aparente (0.089 min^{-1}) da foto-degradação do azul de metileno foi observada na amostra pré-reduzida em árgon a 1300 ºC durante 5 horas e depois oxidada em ar a 400 ºC durante 25 horas, sendo apenas 1.6 vezes menor que a velocidade observada utilizando o pó industrial, nanoestruturado P25 como fotocatalisador, testado nas mesmas condições. As tendências observadas demonstram boas perspetivas para o design de fotocatalizadores multifuncionais à base de titânia baseado na flexibilidade do controlo da composição de fases.

keywords

abstract

This work was focused on designing the phase composition and microstructure of composite rutile – silicon carbide mixture by controlled redox reactions, aiming the preparation of multifunctional titania-based photocatalysts with inherent capabilities for thermal co-activation and stabilization of the anatase polymorph. The materials were processed using a conventional solid state route, involving a partial reduction of the rutile by SiC in inert Ar atmosphere, followed by the post-oxidation in air. The impacts of processing conditions on the phase composition of the oxidized samples and their photocatalytic activity were evaluated using Taguchi experimental planning. The XRD studies confirmed the presence of rutile/anatase mixtures in the oxidized samples. The results emphasized that the pre-reduction and post-oxidation temperatures are the most critical parameters in defining the phase composition, while the post-oxidation time appears to be relevant for the photocatalytic performance. Microstructural studies revealed the formation of core-shell particles in the pre-reduced and post-oxidized samples, which can suppress the photocatalytic activity. The highest apparent reaction rate (0.089 min^{-1}) of the photodegradation of methylene blue was observed for the sample pre-reduced in Ar at 1300ºC for 5 h and then oxidized in air at 400ºC for 25 h, which is only 1.6-times lower than that for nanostructured industrial P25 photocatalyst, tested under the same conditions. The observed trends demonstrate good prospects for designing multifunctional titania-based photocatalysts based on the flexibility of the phase composition control.

Index

List of Figures

List of Tables

List of Abbreviations

	Name	Unit
UV	Ultraviolet	-
CB	Conduction band	-
VB	Valence band	-
h^+	Electron hole	-
e^-	Electron	-
$h\nu$	Photon energy	J
ΔH	Enthalpy	kJ/mol
ΔS	Entropy	J/mol.K
ΔG	Gibbs free energy	kJ/mol
Ar	Argon	-
T_{Ar}	Temperature of reduction	ºC
T_{ox}	Temperature of oxidation	ºC
t_{ox}	time of oxidation	h
SEM	Scanning electron microscopy	-
EDS	Energy-dispersive spectroscopy	-
XRD	X-ray powder diffraction	-
ICDD	International center for diffraction data	-
UV-Vis	Ultraviolet-visible	-
BET	Brunauer-Emmett-Teller	-
K_{ap}	Apparent rate constant of the first-order kinetics	min^{-1}
t	Time	h
$t_{1/2}$	Half-life time of photocatalytic degradation	min
C	Concentration	mg/L
C_0	Concentration at t = 0	mg/L
V_T	Total pore volume	cm^3

1. Introduction

1.1. Heterogeneous catalysis: concepts and mechanisms.

The process of heterogeneous photocatalysis can be described as the acceleration of a photoreaction in the presence of a catalyst. Interest in this area raised when Fujishima and Honda used the photochemical properties of TiO_2 to split water into hydrogen and oxygen [1]. The heterogeneous photocatalytic process is initiated when the photocatalyst, usually a semiconductor, is exposed to photons. These photons excite the electrons at the surface of the photocatalyst. Usually electrons become excited in the valence band, but if the energy of the photons is greater than the band gap of the material used as photocatalyst, the electrons go up into the conduction band [2].

Once the excited electrons move to the conduction band, positive holes with a strong oxidizing character are created in the valence band, as shown in Fig. 1.1.
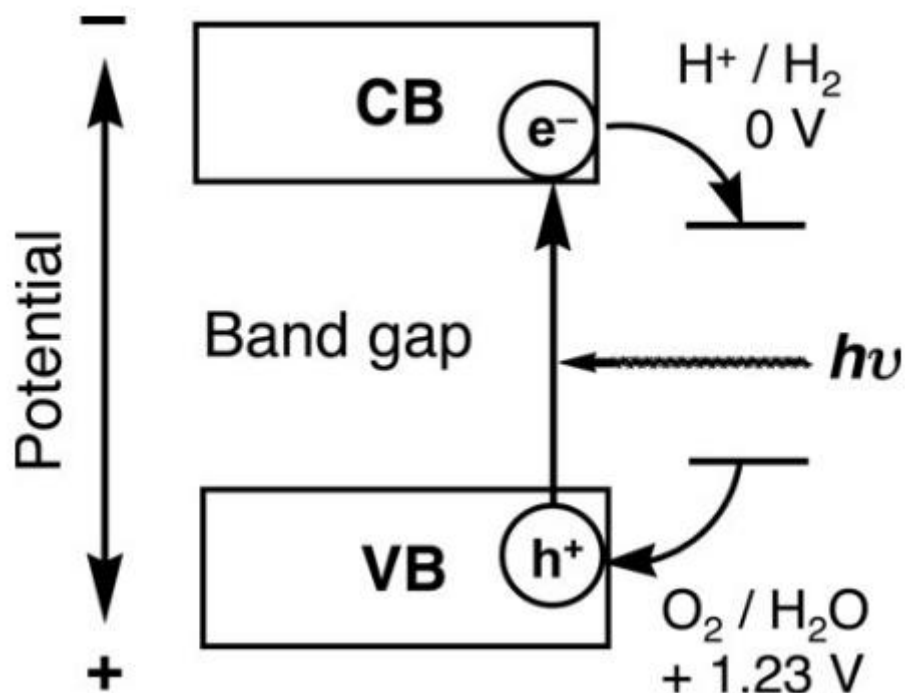
Fig. 1.1 - Mechanism of heterogeneous photocatalysis employing a semiconductor [3].

The excited electrons in the conduction band can react with oxygen (O_2). In the case of using photocatalysis to clean waters, the reaction of the electron with the oxygen creates reactive oxygen species that are then able to oxidize organic molecules in the surface of the catalyst, such as organic pollutants, and to convert them into water (H_2O) and/or carbon dioxide (CO_2) [2].

Most heterogenous photocatalysts are semi-conductors, and the photocatalytic reactions occur in this type of materials as shown in Fig. 1.2. Semiconductors are characterized with a band structure, where the conduction band is separated from the valence band by a band gap with a

suitable width. When the energy of incident light is larger than that of a band gap, the photocatalytic process occurs [3]. The electrons and holes generated cause redox reactions similarly to the electrolysis. Water molecules are reduced by the electrons to form hydrogen (H_2) and are oxidized by the holes (h^+) to form oxygen (O_2) for the overall water splitting. The width of their band gap and the levels of the valence and conduction bands are very important for the photocatalytic activity of a semiconductor material.
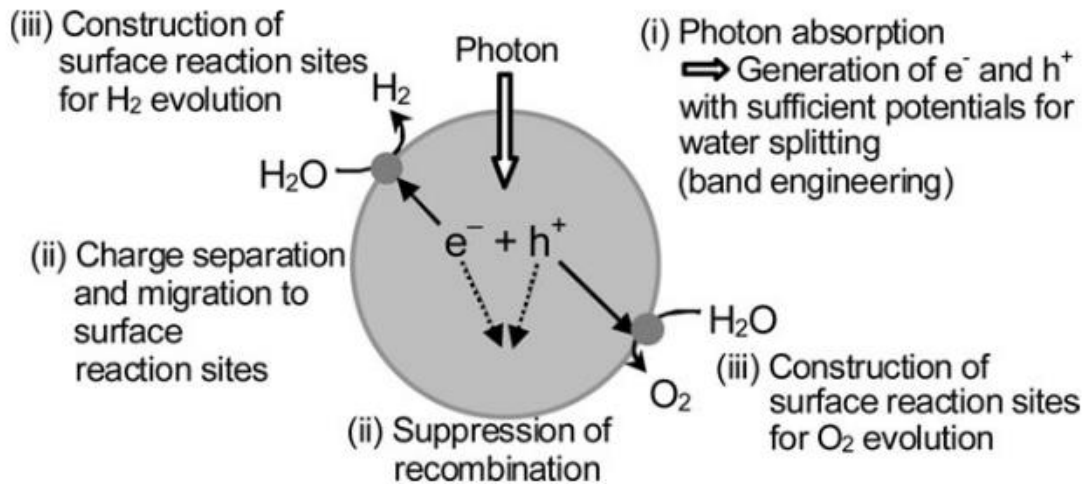
Fig. 1.2 - Main processes in heterogenous photocatalytic water splitting [3]*.*

As depicted in Fig. 1.2, the first step (i) of a photocatalytic process includes absorption of photons to form electron–hole pairs.

The second step (ii) consists of charge separation and migration of the generated carriers. This step can be strongly influenced by crystal structure, crystallinity and particle size. It is important to keep a balance between the crystalline quality and the number of defects. Higher crystallinity implies less defects, and defects operate as trapping and recombination centers between photogenerated electrons and holes, resulting in a decrease in the photocatalytic activity. There should exist a reasonable compromise between the particle size and the surface area, which influences the last step as described below. If the particle size is small, the distance that generated electrons and holes have to migrate to reaction sites on the surface shortens and this results in a decrease in the recombination probability [3].

The final step (iii) depicted in Fig. 1.2 involves the surface chemical reactions. In this case, the concentration of active sites and overall surface area are the crucial parameters. Even if the generated electrons and holes possess thermodynamically sufficient potentials for water splitting, they may recombine without contribution to the photocatalytic process, if the active sites for redox reactions are not sufficiently present at the surface [3].

Platinum is often used as a co-catalyst for water splitting. The co-catalysts are necessary because the conduction band levels of many oxide photocatalysts are not high enough to reduce water to produce H_2 without catalytic assistance, thus being used to introduce active sites for H_2 evolution. Meanwhile co-catalysts are usually unnecessary for oxide photocatalysts when oxidizing water because this time the valence band is deep enough to oxidize water to form O_2 [3].

A promising application of the heterogenous photocatalysis is the photo- abatement of nitrogenous oxides, NO_x. With the rise of NO_x levels in the atmosphere due to pollution, heterogeneous photocatalysis appears as a viable option for NO_x removal from the air. Fig. 1.3

shows the process of heterogenous photocatalysis, using TiO_2 as a catalyst, with a focus on the degradation of NO_x.
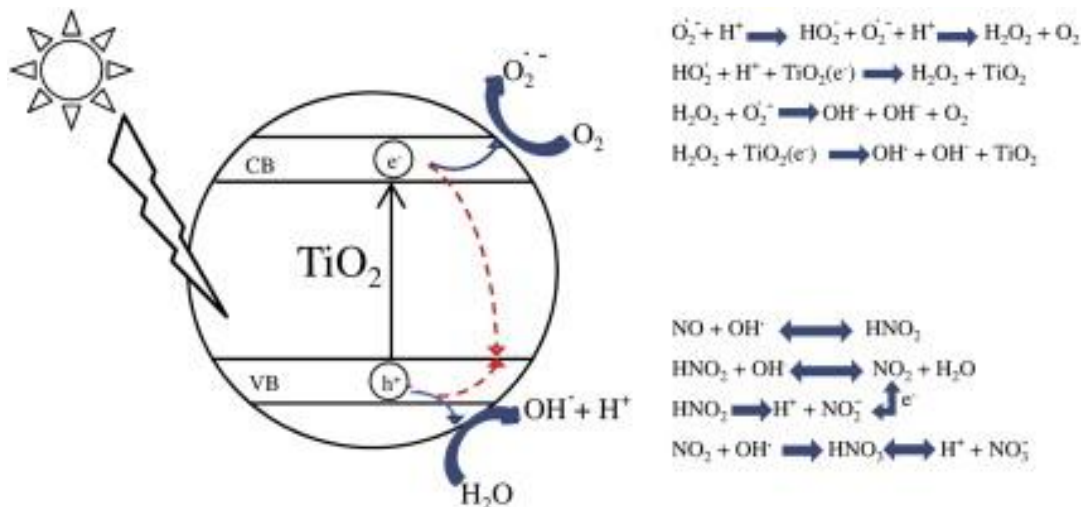
Similarly to the water splitting process, when the catalyst is irradiated by the sunlight it absorbs photons with energy (hv) higher than the bandgap of the semiconductor, generating free electrons in the conduction band according to the equation (1).

$$TiO_2 + hv <-> h^+ + e^- \tag{1}$$
$$h^+ + H_2O_{adsorbed} <-> H^+ + \ {}^\bullet OH \tag{2}$$
$$h^+ + OH^-_{adsorbed} <-> \ {}^\bullet OH \tag{3}$$

Then, holes in the valence band can react accordingly to equations (2) and (3) forming the hydroxyl radicals (•OH). However, at the photocatalyst surface, free electrons and free holes can recombine instead of generating radicals (surface recombination), which strongly limits the photocatalytic activity. The hydroxyl radical reacts with NO, as shown in Fig. 1.3, in several intermediate reactions, ending with the production of H⁺ and NO₃⁻.

The photocatalyzed reactions mentioned above are facilitated through the presence of adsorbed radicals, from water and air, on the photocatalyst surface. The excited electrons (in the conduction band) facilitate reduction of electron acceptor compounds, and the holes created in the valence band act as oxidant of electron donors.

1.2. Materials for heterogenous catalysis.

Photocatalysts have been studied for a long time, since the early 20th century [5]. With the discovery of the water splitting ability of TiO_2, the Honda-Fujishima (1972) [6], research in this topic increased and lead researchers to explore the usage of TiO_2 in many areas especially in photocatalysis [7].

The most used photocatalyst materials are semiconductors, and since the application of TiO_2 for water splitting, more than 130 inorganic materials, like metal oxides, nitrides or sulphides have been tested and considered promising as photocatalyst [8]. Best metal oxides semiconductors in photocatalytic reactions are composed of d^0 or d^{10} orbitals elements like Ti, Zr,

Ga, etc [9]. The conduction band for these metal oxides are usually *d* or *sp*, for d^0 and d^{10} elements respectively, while their valence band is provided by the 2*p* orbitals from the oxygen atoms. In the case of the metal nitrides or sulfides the valence band is provided by the 2*p* orbitals from nitrogen or 3*p* orbitals from sulphur atoms [9].

Fig. 1.4 shows a periodic table with elements constructing heterogenous photocatalyst materials outlined. The elements are classified in four groups [3]:

i) Important for both crystal-structure and electronic band structure;

ii) Important mostly for crystal structure, but less for electronic band structure;

iii) Those forming impurity levels as dopants;

iv) Those used as co-catalysts.

The alkaline earths and some lanthanide ions do not directly contribute to the band formation and construct the crystal structure as A-site cations in perovskite compounds [3].

The transition metals cations with partially filled *d* orbitals, like Cr^{3+} and Ni^{2+}, form some impurity level in band gaps, if they are doped or substituted by native metals cations [3].

Fig. 1.4 - Elements of importance for heterogenous photocatalysis [3].

1.3. Titanium oxides as photocatalysts.

1.3.1. General information and applications.

There has been a lot of research in photocatalysts, however, even with this increased interest in this type of material, TiO_2 remains one of the most investigated photocatalyst [10]. TiO_2 is environmentally benign, biocompatible, abundantly available, highly stable and low-cost metal oxide with the ability to efficiently degrade a wide spectrum of contaminants. Titania can also be immobilized into a variety of supports without losing the photocatalytic activity, thus allowing flexible development of TiO_2 photochemical reactors for air and water purification.

A lot of research works on TiO_2 are focused on shifting its optical response from UV to visible light. Thus, several active TiO_2 materials that utilize some part of visible light of solar radiation for water decontamination were obtained. TiO_2 is already used as a photocatalyst for industrial products like self-cleaning surfaces and anti-fog glasses, Fig. 1.5. However, its use in environmental issues, namely in water remediation, is still not as developed as the applications mentioned earlier [5], being used, in some places, as a tertiary process in waste water treatment [11].
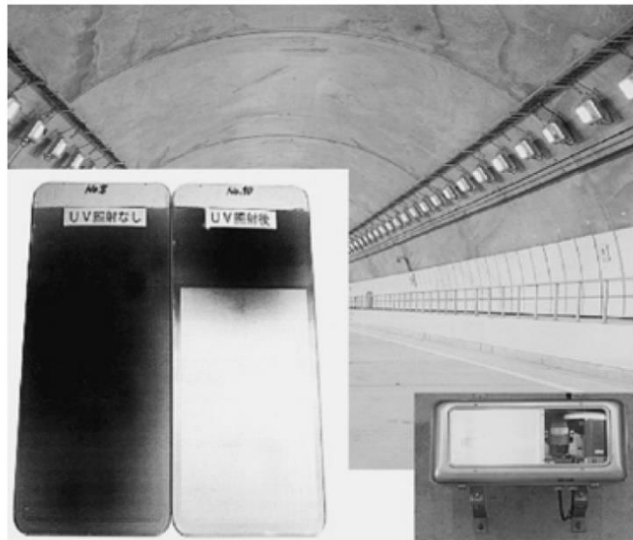
Fig. 1.5 - Glass covers on the highway tunnel lighting shows one darkened by the automobile exhausts without TiO_2 and maintained clean with TiO_2. [5]

However, despite all the benefits of using TiO_2, it presents a major disadvantage. Presently, TiO_2 can only utilize part of the solar irradiation, the UV light (<390 nm), due to its large band gap (anatase = 3,2 eV). UV light makes up only 4-5% of the solar light, while 40% of solar photons are in the visible region [6].

Self-cleaning surfaces

The finding of the photo-induced hydrophilicity has markedly widened the application range of TiO_2 coated materials. Briefly, the stains adsorbed on the titania surface can easily be washed by water, because water soaks between the organic molecules present in the stain and

the highly hydrophilic TiO$_2$ surface. Thus, the TiO$_2$ coated materials used outdoors where they are exposed to rainfall show a very effective self-cleaning function, organics are decomposed partially by the conventional photocatalytic reaction as well as washed by rainwater [5].

Medical applications

TiO$_2$ photocatalysts can be used to kill bacteria [12] and, therefore, self-sterilizing surfaces can be prepared. The ability of TiO$_2$ to disinfect microbes, viruses and bacteria has been put into good used by Japanese researchers. Hospital garments worn by doctors and nurses have "doses" of TiO$_2$ added to the fabric during processing operations to control hospital infections [1]. Photocatalysis has also been used in some developing nations to destroy pathogens and algal blooms [13] in fresh water supplies.

Water purification

Growth in the global population, bigger environmental concerns, and the strong link between water quality and human health require the identification and employment of effective sustainable water treatments to meet the urgent global goal of sustainable clean water. Heterogeneous photocatalysis with TiO$_2$ can be used to treat water supplies due to its capability to oxidize organic compounds such as alcohols, carboxylic acids, phenolic derivatives, oil and convert them into harmless products, for example, carbon dioxide, water, and simple mineral acids [1].

The chances and potential fields of application of photocatalytic systems with artificial UV-sources include new water treatment plants or plants where conventional methods need to be replaced and implemented new ones, based on these new, more advantageous technics.

1.3.2. Main phases and their photocatalytic activity.

Titanium dioxide (TiO$_2$) has three main crystalline phases, which are anatase, brookite and rutile, as shown in Fig. 1.6.

Rutile   Brookite
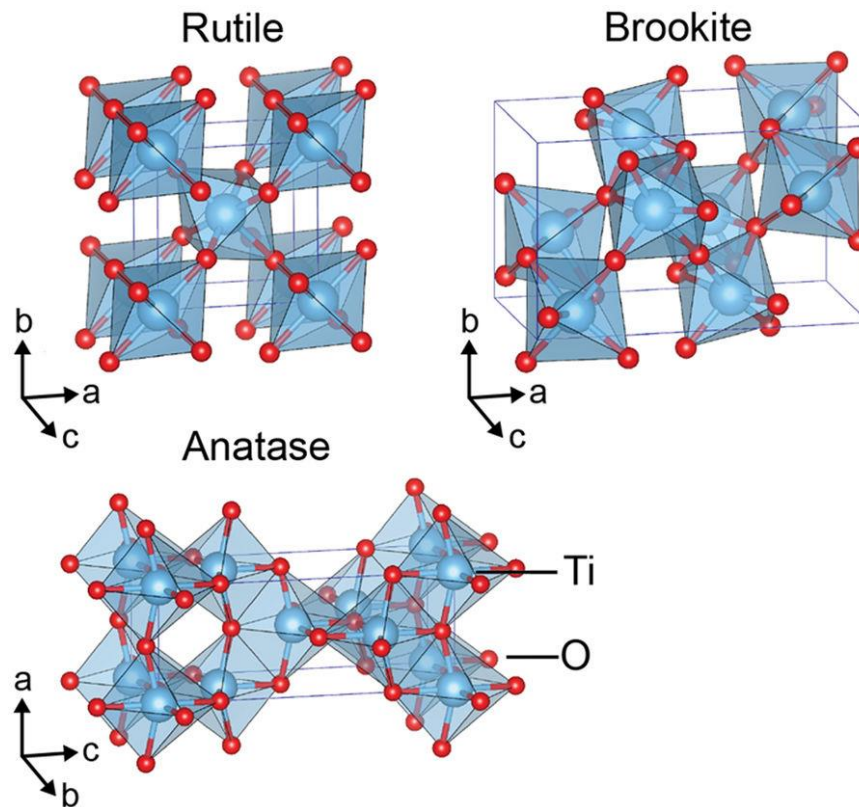
Anatase

Fig. 1.6 - Crystal structures of TiO₂ rutile, brookite and anatase polymorphs. [14]

It has often been reported that the anatase phase is the most active phase in photocatalysis, whereas the effects of the simultaneous presence of rutile (or brookite) are still unclear [15]. Both crystal structures are composed of TiO_6 octahedra, in anatase those octahedra share four edges and only two in rutile, as illustrated in Fig. 1.7. Another aspect of TiO_2-based photocatalysis recently reevaluated is the degree of reduction of the semiconductor. Partially reduced titania crystals (TiO_{2-x}, where typically $0 < x < 1$) induce high photocatalytic rates in wastewater treatment, air purification, hydrogen production by water splitting, and selective oxidation in organic media [16]. However, the stability of Ti^{3+} centers, if these are located at the surface, is generally low.
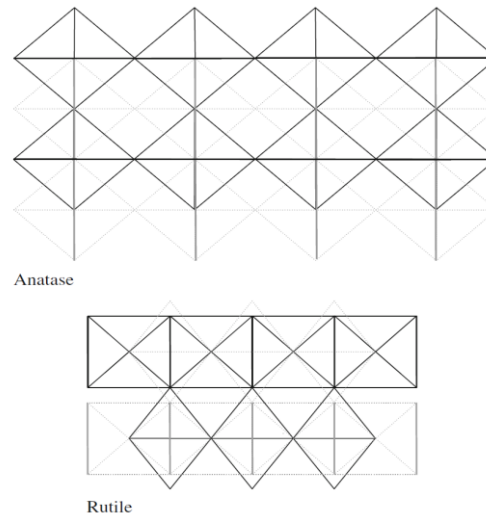
Fig. 1.7 - Two-dimensional projection, down the c-axis, of the TiO₆ octahedra in anatase and rutile, shared edges in bold lines. [10]

There are other forms of reduced titanium with the formula Ti_nO_{2n-1}, where n is a number that ranges from 4 to 10, which are called Magneli phases. These titanium sub-oxides have been investigated due to their high electrical conductivity and chemical stability, which makes them suitable for use in aggressive acidic or alkaline mediums [17]. They also show photo reversible phase transition at room temperature, in case the of Ti_3O_5, which can be used for optical storage. The sub-oxide Ti_4O_7 was found to exhibit high activity and durability for oxygen reduction reaction in aggressive media [18]. Since ultraviolet rays, which can activate an anatase photocatalyst, correspond to less than 4% of solar light, the sub-oxides can be a good alternative to improve the ability of titania to use a greater spectrum of the solar light available. When compared to TiO_2, the Magneli phases can be applied more effectively in cases like the photocatalytic degradation of organic compounds, since they possess a narrower band gap which facilitates the absorption of visible light [19]. There have been developed of several approaches to produce reduced titania crystals, but most of these methods are inconvenient for synthesis of large quantities of reduced titania, required for practical applications.

Despite the larger experimental band gap of anatase of 3.2 eV, compared with 3.0 eV for rutile [20], the photocatalytic performance of anatase generally is considered superior to that of the more stable rutile. This is attributed to a higher density of localized states and consequent surface-adsorbed hydroxyl radicals and slower charge carrier recombination in anatase as compared to rutile; these parameters are crucial for reasonable photocatalytic performance.

The higher rate of electron–hole recombination in rutile is considered to result from typically larger grain size of this material, leading to lower capacity to adsorb species. It is important to note that, owing to the different crystal structures and associated exposed planes of the two polymorphs, anatase has been reported to have a lower surface enthalpy and lower surface free energy than rutile [21]. Hence, it could be expected that the wetting of anatase by water would be less than that of rutile since higher surface free energies generally contribute to hydrophilicity. Due to this higher surface free energy in rutile, one expects a higher density of adsorbed species at its surface, when compared to anatase. Since a high density of adsorbed species would be expected from a hydrophilic material, rutile could be anticipated to exhibit superior photocatalytic performance.

It may be noticed that there are no reports on rutile's exhibiting higher levels of adsorbed species. The photoactivity of anatase and rutile has been examined and interpreted by Sclafani and Herrmann [22], with reference to the densities of surface-adsorbed species. This study

showed that higher levels of radicals adsorbed on the anatase surface gives rise to significantly higher photoactivity than rutile. This result was reported to be due to a higher surface area as well as a higher photoactivity per unit of surface area. A similar result was found by Augustynski [23], who reported that surface-bonded peroxy-containing species on anatase were not present at rutile surface.

In contrast to the widely reported photocatalytic superiority of anatase, several publications have suggested that, in some cases, rutile may be advantageous for certain applications. These studies involved high surface-area rutile of acicular morphology [23], rutile containing residual anatase [24], and iron-doped rutile [25]. It was considered that electron transfer between rutile and a residual quantity of anatase may facilitate improved photo-oxidative reactions, as in mixed-phase titania catalysts. Therefore, considering the importance of surface area, morphology, and doping, an understanding of the titania polymorphs, their transformation, and the methods by which they can be controlled are likely to be critical to achieve the best photocatalytic performance.

It is also noted in some studies that a mixture of anatase/rutile might be better for photocatalysis, when compared with 100% anatase TiO_2 or 100% rutile TiO_2 [26]–[28]. In a research paper, researchers doped TiO_2 photocatalyst to increase the light wavelength absorption and used TiO_2, 100% anatase, and different proportions of rutile/anatase. The photodegradation experiments suggested the mixed-phase TiO_2 exhibited higher photocatalytic activity than that of anatase phase [28]. In another studies the mixed-phase TiO_2 showed the best photocatalytic activity at the rutile ratio of 41.5% [27] and 30% [26], which might show that different proportions might be tested for maximum photocatalytic activity in different applications. It is generally accepted that the presence of rutile introduces mesoporosity and a wider pore size distribution. These factors may be responsible for the increased photocatalytic activity. The photocatalytic activity may represent a combined effect of the pore size, the pore size distribution and the appropriate crystal plane at which the adsorption takes place [26].

1.4. Tailoring phase composition and photocatalytic performance in titanium oxides.

1.4.1. Anatase-to-rutile transformation.

At all temperatures and pressures (Fig. 1.8 and 1.9), rutile is more stable than anatase. This has been confirmed by thermodynamic studies [29], which showed that negative pressures would be required for anatase to be more stable than rutile. Thus, the transformation to rutile is irreversible.
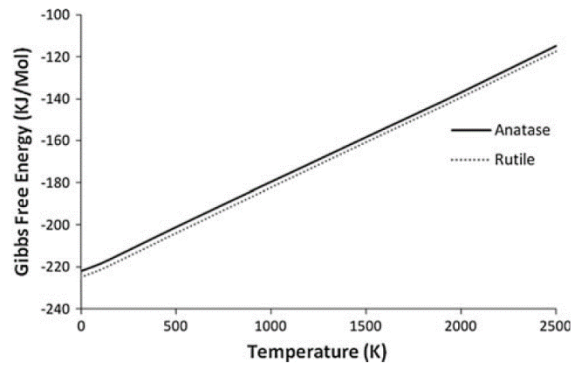
Fig. 1.8 - Plot of Gibbs free energy of anatase and rutile versus temperature. [10]
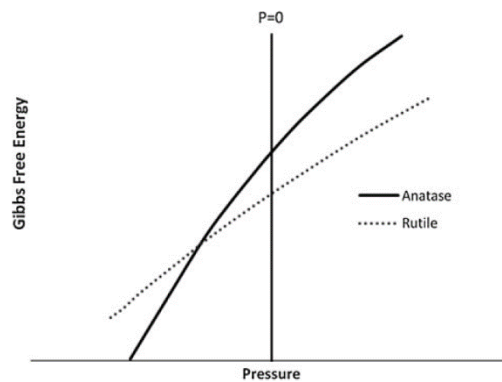
Fig. 1.9 - Schematic plot of Gibbs free energy versus pressure (assumed to be at room temperature). [10]

Table 1.1 shows the reported standard-state thermodynamic data for the anatase to rutile phase transformation.

Table 1.1 - Summary of thermodynamic data from literature (adapted from [10]).

Publication year	ΔH 298 (kJ/mol)	ΔS 298(J/mol K)	ΔG 298(kJ/mol)	Reference
1967	- 5,19	0,42	- 5,32	[29]
1971	- 11,7	0,42	- 11,84	[30]
2009	- 1,70	0,556	- 1,87	[10]

Based on the data in Table 1.1, it appears that some uncertainty still remains regarding the energies of the phase transformation. Over the last 50 years various studies involving kinetics of the transition to rutile have reported various transition temperatures [10]. These studies used different methods to define the phase transformation temperature. As mentioned previously, the temperature at which the transition is observed depends on many parameters and so it is not surprising that a range of values has been reported. However, assessment and consideration of these data lead to the general conclusion that fine powders of high purity show phase transformation at temperatures from 600 to 700 $^{\circ}$C. Excluding studies which used titania of unusually small particle size or long soak times, and studies which did not use onset temperatures as the defined transition temperatures, it can be observed that the reported transition temperatures, as determined by XRD, appear to converge around 600 $^{\circ}$C.

Although it is difficult to ascertain the intrinsic behavior of titania, this is accepted to be the region of the onset temperature of the anatase to rutile transformation in bulk pure anatase in air [10]. This can be seen in Fig. 1.10.
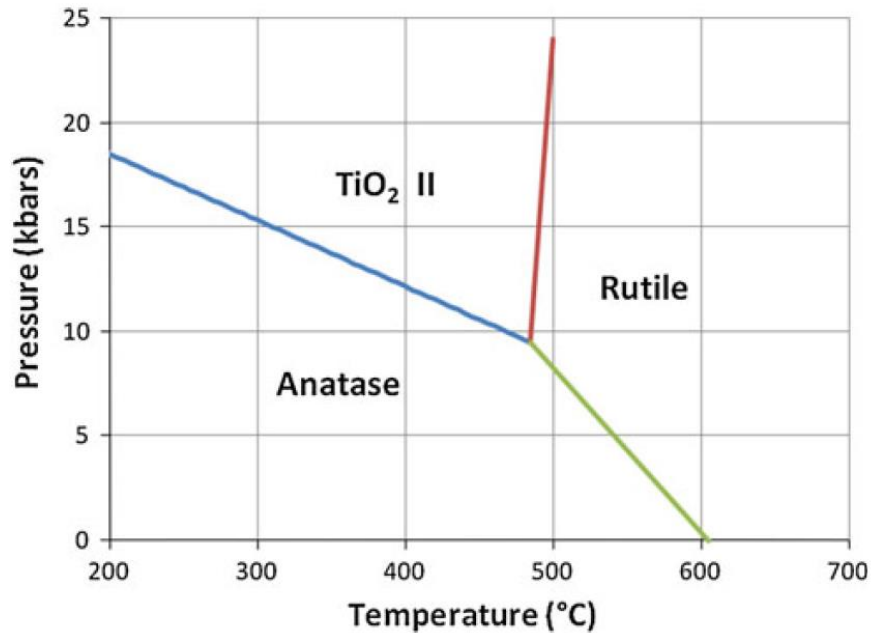
Fig. 1.10 - Reaction boundaries of phase transitions in TiO₂. [10]

Rao [31] studied the kinectics of the phase transformation and the rate of transformation decreased with temperature to a practical limit of 610 ± 10 ⁰C, at which point the transformation became immeasurably slow. Despite the age of this study, it is consistent with later studies [20], [32].

Since rutile corresponds to the equilibrium phase, the presence of anatase demonstrates that these studies cannot represent equilibrium conditions, which normally employ phase diagrams for illustration. Beltrán et al. [20] reported what was a pressure– temperature diagram approximating equilibrium for TiO₂, which is shown in Fig. 1.11. The key observation of these data is the apparent anatase to rutile phase transformation conditions of 605 ⁰C at 1 atm (101 kPa) pressure. The description of this diagram has been subsequently qualified by describing the phase boundaries as reaction boundaries. Current practice is to refer to functional diagrams such as those as behavioral diagrams. Although it is widely accepted that rutile cannot be transformed to anatase, it has been suggested that at high pressures rutile can transform to the a-PbO₂ structured TiO₂ II polymorph [33]. This behavior is outlined by the diagram shown in Fig. 1.11, which is derived from mineralogical samples exposed to high pressures in the earth's crust.
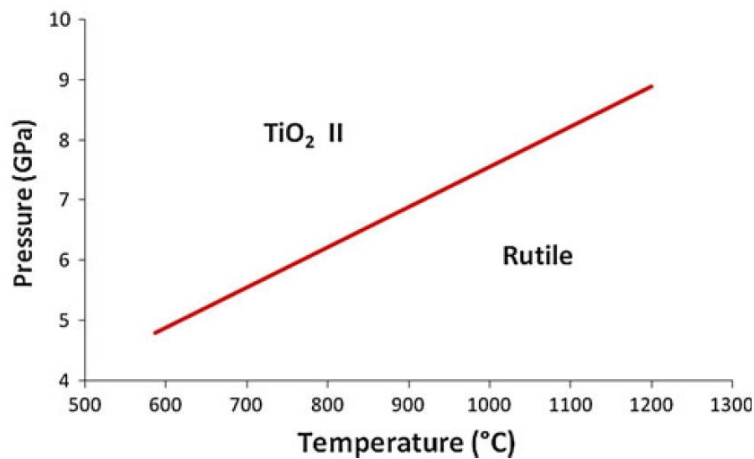
Fig. 1.11 - Proposed behavioral diagram of the transformation of rutile to TiO₂ II. [10]

For the transformation of anatase to rutile proceed at a measurable rate, sufficient thermal energy is required to facilitate the rearrangement of atoms. As described above, it is likely that, for typical bulk titania powders (i.e., not nanoparticles), this energy requirement is reached at 600–700 °C in air in the absence of dopants or impurities, although this is subjective since impurities are always present at a finite level [10]. As will be discussed subsequently, the transformation can be enhanced or impeded by influencing the rearrangement of the atoms in the anatase and rutile lattices. It is perceived widely that the most important factor affecting the phase transformation is the presence and number of defects in the oxygen sublattice [33], [34].

The ease of rearrangement and transformation are enhanced by relaxation (lessening of structural rigidity) of the large oxygen sublattice through the increased presence of oxygen vacancies. This effect has been shown through firing in different atmospheres, where neutral or reducing conditions with low oxygen partial pressure generally greatly enhance the anatase to rutile transformation [34], [35]. This could be a result of reduced heat transfer because vacuum conditions give lower convective heat transfer than air. The promotion of the phase transformation using a reducing atmosphere is considered to be due largely to the increased levels of oxygen vacancies during heating in such atmospheres.

Figure 1.12 shows the effects of different experimental conditions on the kinetics of the anatase to rutile transformation in four different samples. In sample a) titania was doped with Fe_2O_3 in a reducing atmosphere. If it is assumed that the substitution of Ti^{4+} by Fe^{3+} occurs, these substitutions can increase the levels of oxygen vacancies in three potential ways:

(1) the maintenance of charge balance;
(2) spontaneous reduction of Fe_2O_3 to Fe_3O_4 or FeO, which are thermodynamically stable at temperatures as low as 400 °C;
(3) reduction of TiO_2 to TiO_{2-x}.
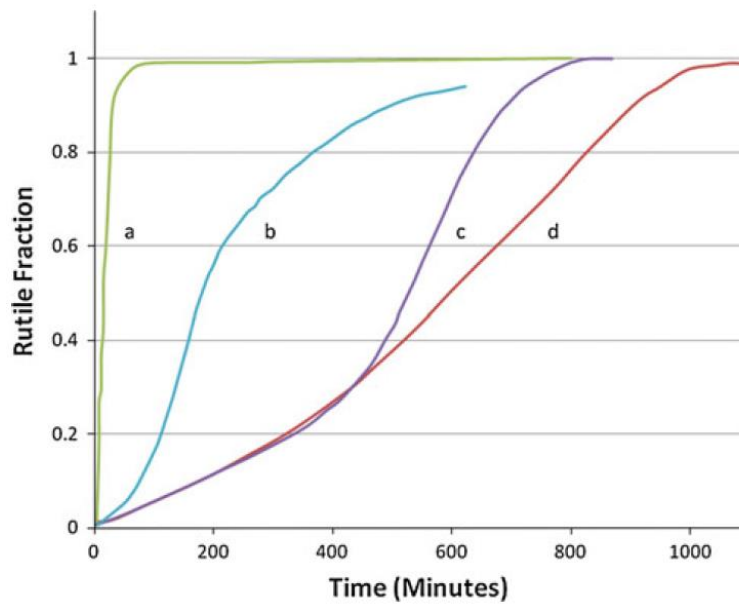
Fig. 1.12 - Time-transformation curves of various titania-based samples. a) Fe_2O_3-doped titania fired in a reducing atmosphere at 1000 ⁰C. b) Undoped titania powder fired in air at 1050 ⁰C. c) MnO_2-doped titania fired in air at 945 ⁰C. d) Undoped titania fired in air at 945 ⁰C. [10]

In the samples b) and d) the only difference is the temperature. Assuming the powders used in the experiments are similar, then it is clear that the phase transformation is accelerated with the use of higher temperature, which is as expected. The effect of doping sample c) with MnO_2, when compared with sample d), is actually similar to the doping with Fe_2O_3, because Mn^{4+} reduces spontaneously in air to Mn^{3+} and then Mn^{2+}, in the assumption of substitution of Ti^{4+} by Mn^{3+} and Mn^{2+}; this results in the generation of oxygen vacancies.

1.4.2. Doping approaches.

In order to improve the photocatalytic activity of TiO_2, many studies have attempted to utilize dopants. In general, the role of dopants includes:

- Reduction of the band gap in titania [36];
- Introduction of mid-gap states [37];
- Improvement in charge carrier separation [38];
- Increase in the levels of surface-adsorbed species, like hydroxyl radicals [39].

The fact that titania may be actually contaminated with some levels of impurities in many cases is not taken into account. The presence of impurities or intentional dopants has strong effects on the kinetics of the anatase to rutile transformation [10]. There have been variable results reported in the sense that dopants can have the effect of hindering or enhancing the transition to rutile. In the case of interstitial solid solution formation, lattice constraint may result in destabilization or stabilization, depending on size, valence, and content effects, again promoting or inhibiting the transformation. If the solubility limit for the impurities or dopants is exceeded, then their precipitation can facilitate the phase transformation through heterogeneous nucleation [34].

Cationic dopants

Numerous cationic dopants have been considered and investigated in terms of their effect on the kinetics of the anatase to rutile transformation. The results suggest that the cations of small radii and low valence accelerate the transition to rutile, due to the increase in oxygen vacancies coming from the substitution of Ti^{4+} ions with lower valences cations [10]. When the cations of valence higher than 4 are employed, their substitution of titanium leads to a lower concentration of oxygen vacancies and formation of Ti interstitials of the same or lower valence.

Through ionic transport, these processes can be viewed considering the inertia to alteration of the relatively large and rigid oxygen sublattice, which largely determines the structural stability and capability to reorganize the chemical bonds to form rutile [10]. Due to this consideration, it is assumed that the substitutional solid solubility leads to the conclusion that small cations of low valence (<4) should promote the transformation of anatase in to rutile, and large cations of high valence (>4) should inhibit it [40]. However, the assumption of substitutional solid solubility may be incorrect and solid solubility occurs [41]. In this case, the insertion of a cation results in the constraint of the required lattice contraction largely in the c direction upon the transformation from anatase to rutile [42]. In this scenario, there is no apparent effect on the charge neutrality. Despite existing reports of interstitial stabilization of the TiO_2 lattice and consequent inhibition of the transformation [10], [42], it appears that there are no reports of destabilization (from structural instability), and consequent promotion of the transformation.

In Fig. 1.13, the formula of the boundary line is:

$$y = -0,0455x + 0,2045 \tag{4}$$

where *x* is the valence and *y* is the ionic radius. In this graph one compares the effects of several dopants for titania, while trying to predict their effect, either as promoters or inhibitors of the phase transformation, based on their ionic radius and valence. As we can see the promoters appear below the boundary line, while the inhibitors appear above the line.
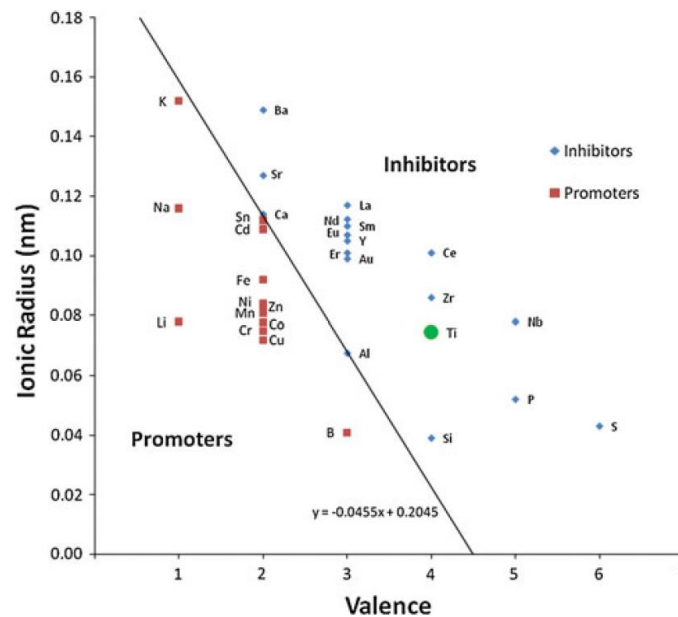
Fig. 1.13 - Comprehensive valence/radius plot of anatase to rutile transformation, categorizing inhibiting and promoting dopants [10].

At the same time, all data shown in fig. 1.13 should be considered indicative owing to the potential presence of impurities and the assumptions stated above.

Studies of the effects of SiO_2 doping on the lattice parameter of anatase also suggested that Si^{4+} enters substitutionally, thereby decreasing the lattice parameter of anatase (and forming interstitial Ti^{4+}) [40], and Tobaldi et al. showed that the addition of SiO_2 to anatase retards the transformation anatase-rutile [43]. In Tobaldi's works it is shown that the transformation anatase-rutile is shifted towards higher temperatures, this is done by the silica added, delaying anatase from reaching the critical size beyond which the phase transformation occurs. However, in terms of photocatalytic performance, the results show that the addition of SiO_2 might lower the photocatalytic activity of the powders due to the formation of an amorphous phase sometimes covering the anatase particles [43]. Yang and Ferreira have also suggested that the contraction observed in the lattice parameters upon SiO_2 and/or doping is evidence of solid solubility [41]. It is possible that the distortion of the lattice by the doping restricts the ionic rearrangement in a similar way as that of interstitial ions. Also, the presence of undissolved SiO_2, possibly as a grain boundary glassy phase, has been suggested to inhibit diffusion and reduce anatase interparticle contact, thus reducing the number of available heterogeneous nucleation sites [40].

Extending the photocatalytic activity of titania

One of the ways discussed that could be used to extend the photocatalytic activity of titania into the visible region is by expanding its band gap or creating mid states in the band gap. This could be achieved using doped TiO_2. It is reported by Tobaldi et al. that the doping with non-metal atoms often had a detrimental effect on the photocatalytic activity of titania because of an enhancement of charge recombination [44].

So the most suitable dopants to improve the photocatalytic activity of TiO_2 might be transition-metals, and rare-earth elements [45]. In fact, Tobaldi et al. showed a shift of the absorption edge of titania, using titania doped powders with WO_3, Nb_2O_5 and La, towards the visible region, demonstrating a way to improve the photocatalytic activity of TiO_2 [45].

Anionic dopants

The doping of TiO_2 using anionic dopants is also of interest due to its significant potential to improve the photocatalytic performance of titania [36], [45]. It is also suggested that anionic doping might have a detrimental effect on the photocatalytic activity of titania due to an improvement in charge recombination [46]. Due to the uncertainty of whether doping actually occurs there is a limited discussion in the literature regarding the effects of foreign anions on the anatase to rutile transformation. However, it is safe to assume that doping by anions results in the filling of oxygen vacancies.

The inhibition or promotion of the phase transformation is likely to depend on size and charge effects, which are as follows [10]:

$$Cl^{1-} > N^{3-} > O^{2-} > F^{1-}$$
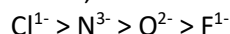
Carbon doping

Carbon is an attractive dopant for titanium dioxide photocatalysts as it has been reported to reduce the band gap and improve photocatalytic performance in anatase [47]. According to equation 4, C^{4+} has an ionic radius of 0,03 nm, which places it close to the line, making it hard to predict the effects of carbon doping on the anatase to rutile transformation based on valence/size considerations. Moreover, there is an apparent absence of reported data regarding the effects of

carbon on the transformation of anatase to rutile. This may be a result of the carbon oxidation at temperatures below the anatase to rutile phase transformation temperature. However, carbon is a very strong reducing agent and, when retained during firing in an inert atmosphere, it would be likely to enhance the transformation to rutile through the formation of oxygen vacancies.

The oxygen-deficient atmosphere created using an inert gas, can also enhance the transformation to rutile through defect formation [34], [35]. In the extreme case, a stable carbide could form by reaction.

Effectively, these are reduction reactions that can contribute in this case:

- Defect formation: $TiO_2 + xC = TiO_{2-x} + xCO$ (5)
- Sub-oxide formation: $TiO_2 + C = TiO + CO$ (6)
- Carbide formation: $TiO_2 + 2C = TiC + CO_2$ (7)

Consequently, carbon is expected to promote the phase transformation, as shown in Fig. 1.14.
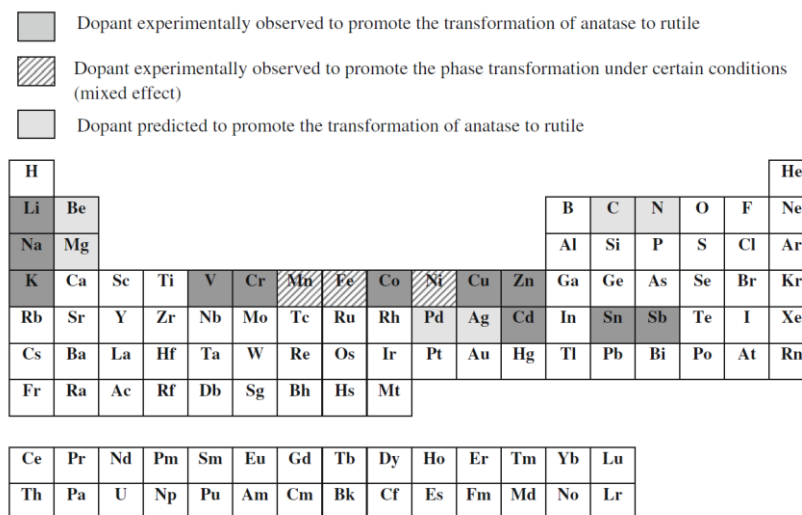
Fig. 1.14 - Experimental and predicted promotion of anatase to rutile transformation based on the preceding considerations. [10]

1.4.3. Effect of the preparation atmosphere.

Rutile is reported widely to exhibit oxygen deficiency and can be described more appropriately as having the formula TiO_{2-x} [48]–[50]. This stoichiometry requires, in principle, the presence of titanium lattice ions, unintentional impurities, and/or intentionally added dopants of valences lower than 4 to maintain charge balance.

This nonstoichiometry may actually be present in anatase as well, although this appears not to have been discussed in the literature. The oxygen vacancies in anatase can be expected to enhance the transformation to rutile owing to the facilitated rearrangement of ions. In contrast to the use of dopants, the atmosphere used during heating of anatase may affect the probability and kinetics of the transformation to rutile. That is, inert (noble gases) or reducing atmospheres (hydrogen) can be expected to increase the number of oxygen vacancies in the anatase lattice

(relative to heating in air), thereby promoting the transformation to rutile. Conversely, heating in air or O_2 can be expected to inhibit the transformation owing to the filling of vacancies [10], [34].

There has been reported the effect of different reaction atmospheres on the anatase-rutile transformation [51]. It has been shown that the type of atmosphere, air, oxygen, argon, nitrogen, affects the rate of transformation anatase-rutile. Reports shows that vacuum and hydrogen atmosphere accelerates the transformation rate while an increase in the oxygen partial pressure decreases the rate of transformation [52]. The explanation proposed by authors is that the formation of oxygen vacancies, favored while using chemically reducing atmospheres, accelerate the transition, while the formation of interstitial Ti^{3+}, usually in vacuum, inhibits the transformation [53]. It is proposed that the formation of oxygen vacancies in the anatase lattice favors bond rupture and the diffusion necessary for the crystal structure rearrangement.

The number of defects created can act as color centers, because with the increase in non-stoichiometry TiO_2 color can change from white to light yellow, grey or even dark blue. The use of reducing atmospheres can also shift the luminescence emission of the TiO_2 powders. It has been shown that a sintering treatment in argon leads to a decrease of the luminescence intensity [54].

1.5. Application of Taguchi planning for materials design.

Experimental design is widely used to optimize the values of various process parameters and aims to improve the quality of a given product. Conventional methods for experimental design often require a large number of experiments, while the number of process parameters can be also significant, especially in the modern industry. Taguchi methods represent a statistical approach developed to enhance the quality of manufactured goods. Recently, it was also applied to engineering, biotechnology, marketing and advertising.

The Taguchi method for experimental design is a great tool to apply to many engineering problems as it allows the analysis of a high number of variables without a high amount of experiments [55]. Taguchi's optimization technique is unique and powerful and allows optimization with minimum number of experiments. The advantages of Taguchi method over other methods are that numerous factors can be simultaneously optimized, and more quantitative information can be extracted from fewer experimental trials [56].

The Taguchi method uses a standard orthogonal array to evaluate the effects of design variables on the response value [57]. Usual steps of the Taguchi experimental design include:

- selection of the output variables or responses to be optimized;
- identification of the factors, or input variables, which affect the output variables;
- determination of the levels of these factors;
- selection of an appropriate orthogonal array;
- assigning factors and interactions to the columns of the array;
- performing experiments, while ensuring a maximum randomizing of the trials to minimize the systematic error;
- analysis of the results, including, when necessary, signal-to-noise ratio analysis;
- determination of the optimal process parameters;
- performing reproducibility experiments, if necessary [58].

The use of orthogonal arrays minimizes the number of total experimental runs such that the conclusions drawn from small scale experiments are valid over an entire experimental region spanned by the control factors and their settings [59].

Usually it is assumed that the effects (individual or main) of each independent variable on the results are separable, which means that no different level of any variable affects the performance of other variables in the process.

The analysis of the results with the Taguchi method is made by applying a statistical measure of performance, signal to noise (S/N) ratio. The signal to noise ratio takes in account both the mean and the variability and depends on the criterium decided for the quality characteristic to be optimized. After the S/N ratio statistical analysis a method of analysis of variance is used for estimating error variance and the determination of the relative importance of each factor [59].

The Taguchi method also employs a multivariate least square fitting model. This model applies the equations that follow:

$$P = f(x, y, z) \approx \theta - \alpha x - \beta y - \gamma z \tag{8}$$
$$\varepsilon = \sum \{P_i - \theta - \alpha_1 x_i - \beta y_i - \gamma z_i\}^2 \tag{9}$$
$$\text{with } \frac{\partial \varepsilon}{\partial \theta} = 0; \frac{\partial \varepsilon}{\partial \alpha} = 0; \frac{\partial \varepsilon}{\partial \beta} = 0; \frac{\partial \varepsilon}{\partial \gamma} = 0$$

where x, y, z are the process parameters, Θ, α, β and γ are the coefficients to be optimized, and P is one of the output variables or responses. In many cases, a correlation matrix, showing correlation coefficients between variables, is used as a way to summarize the data and show the relevance of the selected parameters for adjusting the response.

Since the Taguchi experimental design is expected to reduce costs, improves quality, and provides robust design solutions [56], it is being used in a whole range of areas, or disciplines. This method is particularly important for research, where the impacts of various experimental conditions on the target properties can be analyzed without undue number of experiments, especially when they are sophisticated, time consuming or expensive. As an example, Sanches et al. [60] have reported the use of the Taguchi method to study the effects of processing parameters on cellular ceramics. Studies were also reported on optimization to adjust particle size distributions by wet comminution of bioactive glass [61]. The optimization of the process parameters for the removal of copper and nickel by growing Aspergillus sp. as been reported by Pundir et al. [56]. An example of industrial use of this method is described by W.H. Yang et al. [62], where the Taguchi method was implemented to optimize the cutting task scheduling and resource allocation on cloud computing, as it is described by Jinn-Tsong Tsai et al. [63].

1.6. Motivation and main objectives

This master thesis is related to the project Smart Green Homes project (POCI-01-0247-FEDER-007678), coordinated by the company BOSCH Termotecnologia, within the scope of the activities of the development line LD2-Gas heating, with the emphasis on the catalytic elimination of NO_x and other polluting gases. Titania was one of the materials chosen for these developments, combining photocatalytic activity with other advantageous characteristics, including moderate cost, absence of negative impacts on health, environment or safety, versatility in processing, etc.

There is an extensive list of bibliographical references whose objective is to optimize the photocatalytic activity of titania, often using additives that inhibit the anatase-to-rutile transformation to relatively high temperatures, in order to guarantee the flexibility in the ceramic processing of material based on TiO_2. Alumina and silica are some of the most studied additives, because they inhibit the transformation of anatase, because they retard grain growth of anatase, or even because they allow a decrease of the band gap, favouring the use of a wider spectrum of sunlight.

Thus, the main objectives of this dissertation are to obtain photocatalysts based on redox-transformed TiO_2+SiC mixtures, containing anatase and silica. The choice of silica as a secondary phase is determined by its inhibitory effect on anatase transformation and also because it is one of the main components of conventional ceramics. The presence of silicon carbide (SiC) may allow the self-heating of the catalyst by microwave, combining the photocatalytic activity with thermal co-activation.

An innovative methodology based on the processing of target composites by controlled partial reaction between SiC and TiO_2 is proposed. The precursors were prepared by partial oxidation of SiC and formation of Ti_2O_3 and TiOC phases. The final functionalization was carried out by oxidation at intermediate temperatures, to favour the formation of anatase, with the contribution of silica to minimize the transformation in rutile. The processing steps were controlled and characterized by X-ray diffraction analysis and microscopy studies based on combined SEM/EDS. Finally, the photocatalytic activity of the prepared materials was evaluated through photodegradation tests of a model organic pollutant, carried out in a laboratory photo-reactor.

The objectives of this thesis include:

- Demonstration of the concept for preparation of TiO_2+SiC+SiO_2 composites containing anatase by solid state processing, involving pre-reduction and controlled oxidation;
- Identification of the processing conditions, which promote the formation of a greater amount of anatase;
- Evaluation of the structural and microstructural evolution during the processing stages;
- Performing photocatalytic tests based on the oxidation of organic dyes using the prepared composite materials;
- Establishing general guidelines for the processing routes that result in enhanced photocatalytic performance.

2. Experimental

2.1. Processing of the composite samples

The precursor powders for preparation of the target composite materials included titanium (IV) oxide, rutile (TiO_2, Alfa Aesar, Kandel, Germany) and silicon carbide, β-phase (SiC, Alfa Aesar, Kandel, Germany). These powders were mixed in a molar proportion of 1:1, and ball-milled with alcohol, using nylon container with Tosoh tetragonal zirconia milling media, for 4 hours at 50 rpm. After drying, the mixed powders were used for the preparation of 10mm-thick pellets by uniaxial pressing at ≈40 MPa during ≈30 s. The weight of the powder used for each pellet was kept constant at around 1.2 g. After compacting, the pellets were sintered in inert Ar atmosphere and further partially re-oxidized in air to assess the possibility for formation and maintaining various titania-based phases for improved photocatalytic activity.

In order to understand the effect of the processing conditions on phase composition and photocatalytic activity, a Taguchi plan was implemented, involving three variable parameters, namely, the temperature of sintering in Ar (T_{Ar}), and the temperature (T_{ox}) and time (t_{ox}) of re-oxidation, which was expected to be crucial for the anatase formation. This route is shown in Fig. 2.1.
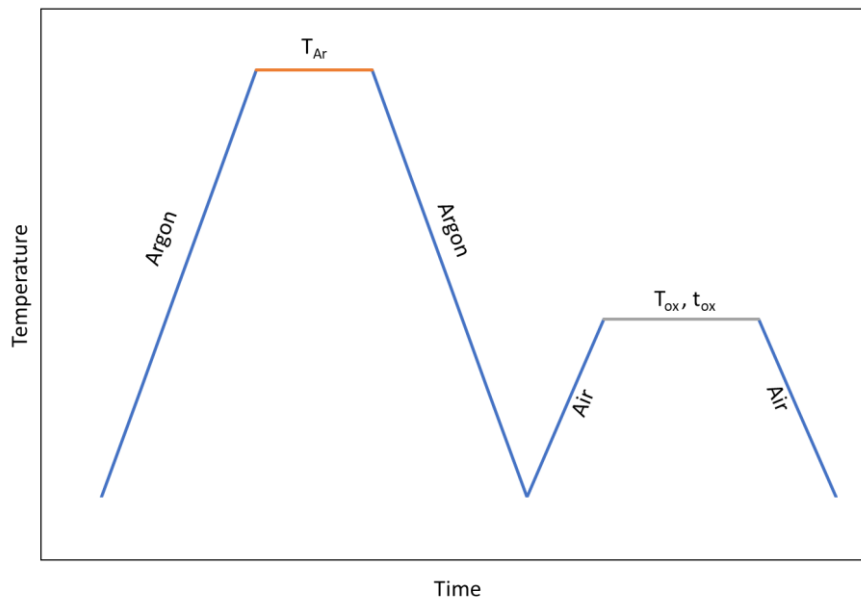
Fig. 2.1 - Qualitative diagram of the thermal treatment procedure used for the preparation of composites.

Firstly, the rutile and silica were reacting in quasi-inert, or mildly reducing Ar atmosphere to prevent full oxidation. Three different temperatures (T_{Ar}), namely, 1250, 1300 and 1350 °C, with a fixed heating rate of 5.0 °C/min, a fixed dwell of 5 hours and a fixed cooling rate of 5.0 °C/min were used. At second step, the ceramic samples after treatment in Ar, were subjected to the thermal treatment in air atmosphere at lower temperatures (T_{ox}, t_{ox}), aiming at least partial formation of anatase. The time scale for dwell was selected assuming typical logarithmic

dependence of the oxidation rate on time. Table 2.1 and Table 2.2 show the orthogonal array of the corresponding processing conditions based on the Taguchi method previously described.

Table 2.1 - Variables and levels used in this study with the Taguchi method.

Levels	Variables		
	Temperature of reduction (T_{Ar}) #1	Temperature of oxidation (T_{ox}) #2	Time of oxidation (t_{ox}) #3
1	1350 (1)	500 (1)	25 (1)
2	1300 (2)	450 (2)	5 (2)
3	1250 (3)	400 (3)	1 (3)

Table 2.2 - L_9 orthogonal array of the processing conditions used Taguchi planning.

Experiment	T_{Ar}, °C	T_{ox}, °C	t_{ox}, h
E1	1350	500	25
E2	1350	450	5
E3	1350	400	1
E4	1300	500	5
E5	1300	450	1
E6	1300	400	25
E7	1250	500	1
E8	1250	450	25
E9	1250	400	5

The Table 2.3 lists the denominations of other samples, used for comparative studies.

Table 2.3 – Denominations of the samples, used for comparative studies.

Sample denomination	T_{Ar}, °C
IM	− (initial mixture)
1250Ar	1250
1300Ar	1300
1350Ar	1350

2.2. Characterization

2.2.1. Quantitative and qualitative phase analysis by XRD

The XRD analysis is based on the physical phenomenon of constructive and destructive wave interference. The interference of the monochromatic X-rays, generated by a cathode ray tube and filtered, and the crystalline sample produces constructive interference when conditions satisfy Bragg's law (nλ=2d sin θ). This mathematical law relates the wavelength of the electromagnetic radiation to the diffraction angle and the lattice spacing in a crystalline sample. This interaction provides a generated pattern and a unique fingerprint of the crystal presents in the sample.

The Rietveld refinement technique, with the XRD pattern can also be used for the characterization of crystalline materials. This technique takes into consideration the height, width and position of the reflections present on the XRD pattern, to determine many aspects of a material structure like the crystalline phases present in the sample. This method uses a least square approach to refine a theoretical line profile until it matches the measured XRD pattern.

For the XRD analysis, the samples were prepared in a powdered form, using an agate mortar to grind part of the ceramic pellet after treatment in Ar and post-oxidation. The qualitative phase analysis of the sample was done using a high-resolution diffractometer (Malvern PANalytical X'Pert, Worcestershire, United Kingdom) with a radiation Cu Kα (I=1.540598 Å), Fig. 2.2. The acquisition of the data was done with a scan interval of 5 to 80°, with ½ and ¼ slits and a 200 seconds step time. The identification of the crystalline phases was done by comparing the diffractogram obtained with standard diffractograms of the respective crystalline phases detected, using the equipment-associated software.

Fig. 2.2 - High-resolution diffractometer used to collect the data.

The quantitative analysis of the crystalline phases was obtained using the Rietveld refinement method (TOPAS Version 4.2, Bruker AXS, Karlsruhe, Germany). The selected ICDD

numbers for the powder analysis were: #04-005-8760 for Ti_2O_3, tistarite, #04-016-0561 for TiO_2, rutile, #01-075-2546 For TiO_2, anatase, #01-074-2307 for SiC, β-phase, #04-008-7640 for SiO_2, cristobalite and #04-002-5443 for TiCO.

2.2.2. Microstructural analysis using SEM and EDS

The scanning electron microscope analysis (SEM) uses a focused beam of high-energy electrons to interact with the surface of the samples. Those signals that derive from the electron sample interactions unveil information like the external morphology, chemical composition, crystalline structure and orientation of the materials making up the sample. SEM often has an EDS (Energy Dispersive x-ray Spectroscopy) system integrated in the instrument.

The EDS system consists of a sensitive X-ray detector, liquid nitrogen for cooling, and software to collect and analyze the data gathered. An EDS detector uses a crystal to absorb the energy of the incoming x-rays by ionization, yielding free electrons in the crystal become conductive and produce an electrical charge bias. The energy of individual x-rays is them converted into electrical voltages of proportional size that correspond to the characteristic x-rays of the element present.

In this work, the combined SEM/EDS studies were performed using both fractured ceramic samples and powders, prepared by accurate destroying of the ceramics without excessive grinding. The samples used for SEM/EDS analysis were prepared placing a portion of the powder in carbon tape on alumina holder; in the case of ceramic samples a carbon glue was used to fix them on the holder. The samples were then submitted to carbon deposition (Carbon Evaporator K950, Emitech, France).

The microstructural studies were performed using SEM - Hitachi SU-70 instrument, to inspect relevant microstructural features and their evolution depending on the processing conditions. Complementary EDS analyses were performed for the same samples using Bruker Quantax 400 detector, to confirm the phase composition and assess the distribution of various phases.

2.2.3. BET surface area analysis

Nitrogen physisorption experiments were performed with a Gemini V2.0 Micromeritics Instrument (Micromeritics, Norcross, GA, USA) to investigate the specific surface area and porosity of the materials. The specific surface area was calculated from the N_2 adsorption data using the BET (Brunauer-Emmett-Teller) method [64]. This method involves the determination of the amount of adsorptive gas (N_2) required to cover the external and the accessible internal pore surfaces of the solid with a complete monolayer. The monolayer amount can be calculated from the adsorption isotherm using the BET equation 10,

$$\frac{p/p_0}{n_a \left(1 - p/p_0\right)} = \frac{1}{n_m C} + \frac{C-1}{n_m C} \frac{p}{p_0} \tag{10}$$

where n_a is the specific amount of N_2 adsorbed at the relative pressure p/p_0, n_m is the specific monolayer N_2 amount and C is the BET parameter. Both n_a and n_m are expressed in mol/g. The BET equation is usually applied to relative pressures between 0.05 and 0.3.

The specific surface area per mass of the sample, S_{BET}, is calculated from the monolayer amount (n_m) using equation 11, by assessing a value for the average area occupied by each molecule (a_m) in the complete monolayer.

$$S_{BET} = n_m \, a_m \, N_A \tag{11}$$

The average area of a N_2 molecule at 77.3K is 0.162 nm^2 [64]. Considering the value of the Avogadro constant ($N_A = 6.022 \times 10^{23} \, mol^{-1}$), equation 11 becomes:

$$S_{BET} = 9.76 \times 10^4 \, n_m \tag{12}$$

where n_m is expressed in mol/g and S_{BET} is expressed in m^2/g. The total pore volume (V_T) was defined as the volume of liquid nitrogen corresponding to the amount adsorbed at a relative pressure $p/p_0 = 0.99$ (Gurvitch rule) [65].

2.2.4. Photocatalytic tests

The system used to perform the photocatalytic test is as presented in Fig. 2.3. Fig. 2.3-1, provides the cool water to control the temperature by circulating it in the photoreactor, Fig. 2.3-2. To keep the particles in suspension during the test, a magnetic stirrer plate with a magnet in the solution was employed, Fig. 2.3-3. Due to the use of ultraviolet light as a radiation source, Fig. 2.3-5, and its dangers the photoreactor was protected with an aluminium cylinder, Fig. 2.3-4.

Fig. 2.3 - Experimental setup to perform photocatalytic tests.

In this experiment methylene blue (Riedel-de Haen, methylenblau B extra for microscopy) was used as organic dye, degrading depending on the photocatalytic activity of the sample. The reference photocatalytic powder, 80% anatase and 20% rutile, used in industry, with good photocatalytic performance (Aeroxide, TiO_2 P25, Evonik Industries, Hanau, Germany) was also tested to compare the performance with composites studied in the present work. The photocatalytic properties of the powders were analysed using a methylene blue solution, a reactor consisting of a flask, Fig. 2.4-(1), an quartz immersion well, Fig. 2.4-(2) and a UV lamp Fig. 2.4-(3), as shown in Fig. 2.4.
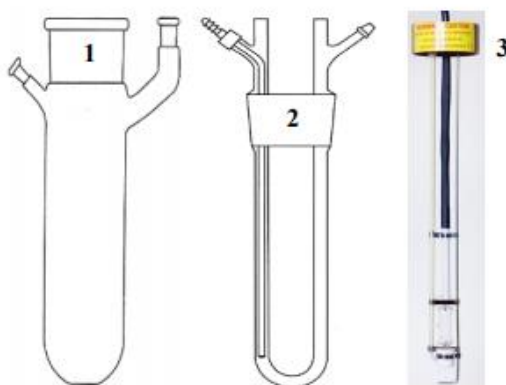
Fig. 2.4 - Schematic of the photochemical reactor used. (1) Standard flask; (2) Immersion well; (3) UV lamp.

The reactor has a capacity of 200 ml of solution and the lamp used had a potency of 0.515 W.
The methylene blue solution concentration was 10 mg/l. The volume of solution for the reaction used was 200 ml and the amount of photocatalytic powder used was 0.1 g. The tests lasted 2 hours and 20 min, with the methylene blue solution. Tests consisted in the first hour being dark to let the concentration of the solution stabilize due to surface adsorption of methylene blue molecules onto the powder. The aliquots (4 ml each) were taken every 10 min after the dark hour and centrifuged for 5 min to remove the powder before being stored for analysis. During the teste, to keep constant temperature of about 15 to 20 °C, one used a circulating water system, with ice, to keep the solution around the desired temperature.

The aliquots were analysed to measure their absorbance with an ultraviolet-visible spectrophotometer (GBC, Cintra 303). The acquisition of the data was done using the software Cintral, and the conditions used included a scan interval of 800 to 300 nm, with a speed of 200 nm/min, a step size of 0.480 nm and a slit width of 2.0 nm. The reference used was distilled water.

The concentration of methylene blue in aliquots taken was calculated based on the Beer-Lambert law, shown below equation 13:

$$A = \varepsilon \times b \times c \tag{13}$$

were A is the absorbance, ε is the molar absorptivity (L/mg.cm), b the path length of the sample (cm) and c the concentration of the sample (mg/L). In order to perform this analysis, the calibration curves were created for the methylene blue solutions. For fixed known concentrations of the dye, the absorbance was measured in quartz cuvettes 1 cm width (b=1 cm); in this way the absorbance at maximum absorption peak (664 nm) was plotted against the concentration, as shown in Fig. 2.5 and Fig. 2.6, with a good linear correlation.
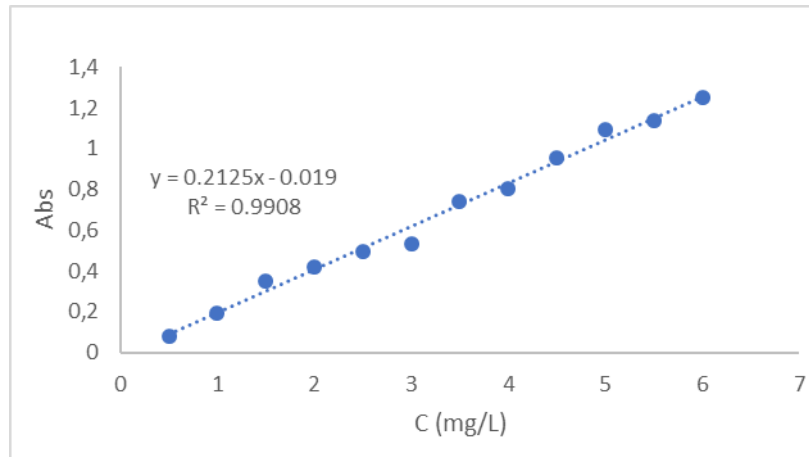
Fig. 2.5 - Calibration curve for the methylene blue solutions, with a linear regression and the respective equation.

Using a linear regression, we obtained an equation for calculating the concentration methylene blue, equation 14, at different stages of the photocatalytic tests:

$$y = 0.2125x - 0.019 \tag{14}$$

were x is the concentration of the sample and y, the measured absorbance at 664 nm. Since methylene blue can degrade by photolysis in the conditions with only light without photocatalyst in a reference test, one compared the rate at which the photolysis occurs and the photocatalytic performance of prepared composites. The results are shown in Fig. 2.6.
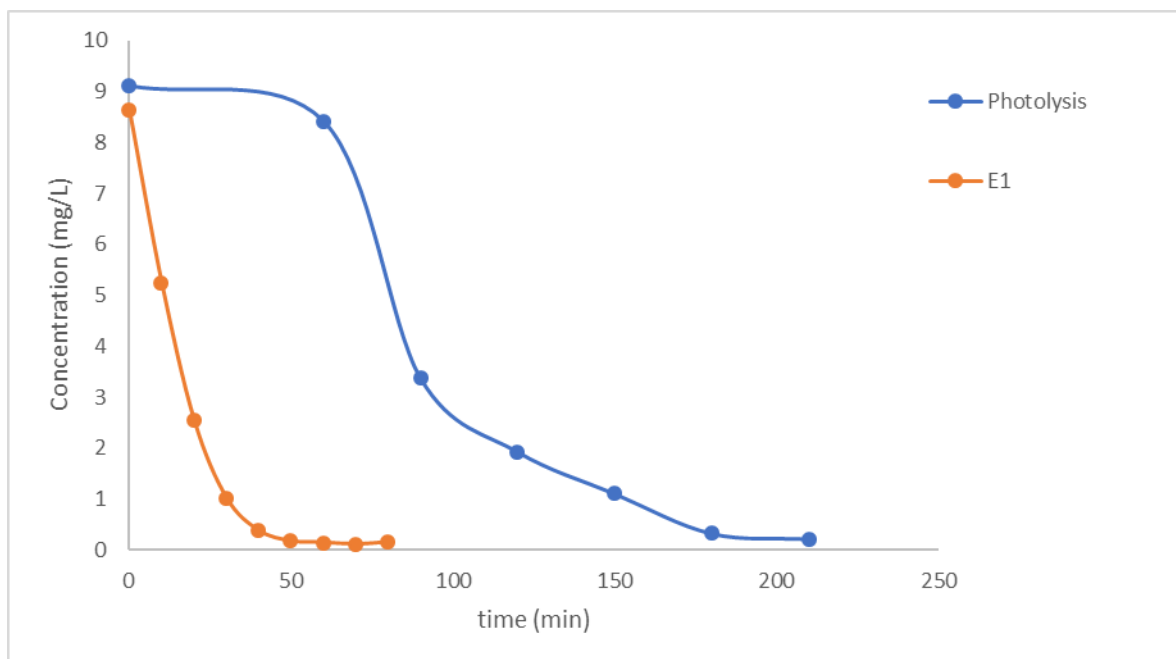
Fig. 2.6 - Comparison of the degradation rate of methylene blue in the absence of photocatalyst (photolysis) with one exemplary photocatalytic test with the composite powder.

One can notice that, in the presence of prepared composite photocatalyst, the degradation of the methylene blue takes place significantly faster. Thus, such experiments allow to attribute the

changes in the concentration of methylene blue along the time to the inherent photocatalytic activity of the prepared composite powders.

3. Discussion

3.1. Processing effects on the phase composition

The selected processing route for the preparation of titania-based composites included the powder pressing as one of the steps and further sintering of the ceramic samples. From the first look, this approach does not appear to be optimal for processing materials suitable as photocatalysts, where nanostructuring and large available surface area are usually required [66]. However, the selected method allowed to provide a better contact between the rutile and SiC particles during the reaction and to minimize surface oxidation of silicon carbide without reaction with titania. In order to avoid ambiguities arising from intermediate ceramics grinding, both steps of processing in quasi-inert Ar atmosphere and post-oxidation were done for ceramic samples. Preliminary tests showed that the selected range of processing conditions does not result in excessive densification (the ceramic samples were porous enough to soak water). Thus, sufficient open porosity of Ar-processed samples was provided.

The XRD results obtained for the samples processed in Ar atmosphere are shown in Fig. 3.1.
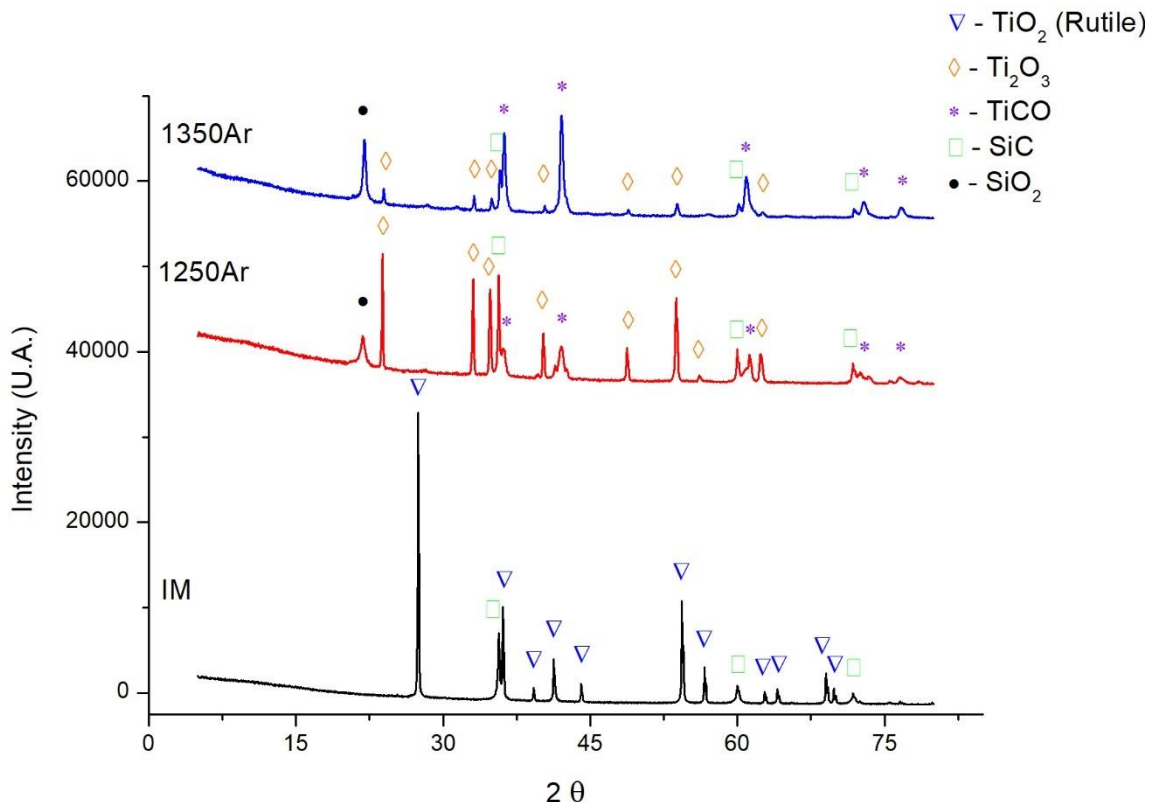
Fig. 3.1 - Comparison of the XRD results obtained for initial powder mixture and 2 samples processed in Ar atmosphere at different temperatures.

The results depict significant changes in the phase composition after processing in Ar as compared to the initial mixture. The formation of at least three new phases, including reduced titanium

oxide Ti_2O_3, titanium oxycarbide TiOC and silicon oxide SiO_2, was observed. The results of the XRD quantification are given in the Table 3.1 and 3.2.

Table 3.1 - Phase quantification in the samples processed in Ar at different temperatures.

Phase	Ar-processed samples, % mol.		
	1250Ar	1300Ar	1350Ar
Ti_2O_3	22.2	13.9	4.9
TiO_2 (rutile)	–	–	–
TiO_2 (anatase)	–	–	–
SiC	40.9	27.7	17.6
SiO_2	21.1	26.5	34.9
TiCO	15.8	31.9	42.6

Table 3.2 - Phase quantification in the samples processed in Ar and post-oxidized in air.

| Phase	Oxidized samples, % mol.								
	E1	E2	E3	E4	E5	E6	E7	E8	E9
Ti_2O_3	–	3.4	4.6	5.1	11.9	9.5	15.4	10.2	26.2
TiO_2 (rutile)	40.1	30.1	22.4	39.4	27.1	26.2	23.3	29.2	1.7
TiO_2 (anatase)	7.8	12.6	19.2	0.9	2.1	8.4	1.6	1.5	1.8
SiC	17.9	19.8	20.1	26.0	30.6	28.6	41.6	41.3	49.4
SiO_2	34.1	34.1	33.8	28.6	28.3	27.3	18.1	17.8	20.9
TiCO	–	–	–	–	–	–	–	–	–

In this table, the quantitative results in % wt. obtained by Rietveld refinement of the XRD data were converted to % mol. in order to better illustrate the reaction stoichiometry. It should be noticed that the nominal molar Ti/Si ratio of initial mixture (1:1) is kept at acceptable level in the results of the XRD quantification. As an example, in accordance with the results presented in the Table 3.1, this ratio corresponds to 0.97, 1.09 and 0.98 in the case of the samples 1250Ar, 1300Ar and 1350Ar, accordingly. The latter is a good confirmation of the quality of the XRD quantification and its relevance for the analysis of phase transformations observed in the present work.

In general, assuming the observed phase composition, the reaction between titania and silicon carbide can be represented as follows:

$$3TiO_2 + SiC \rightarrow Ti_2O_3 + TiOC + SiO_2 \tag{15}$$

The formation of titanium oxycarbide by carbothermal reduction of titania in inert or CO-containing atmospheres at the temperatures similar to those employed in this work was previously observed in many studies (for example, [67], [68]). In agreement with the cited papers, higher temperatures of the treatments in Ar increase the fraction of TiOC formed, corresponding fraction of SiC decreases with the temperature increase. The deviations of TiOC to SiO_2 molar ratio from 1:1, predicted in accordance with the Eq. (15), can be attributed to the partial oxidation of silicon carbide by oxygen residues presented in Ar and possible presence of the amorphous phase. In general, the results suggest that the extent of the reaction between rutile and silicon carbide can be well-controlled by sintering conditions. Although the time of Ar treatments was not varied in this work, kinetic control of this reaction under discussed conditions is expected to allow flexible tuning of the phase composition and residual amount of SiC phase, if the latter is required for thermal co-activation of the catalyst by the microwave irradiation.

The pre-processing in Ar atmosphere allowed to attain two prerequisites for further anatase formation and stabilization, aiming tunable photocatalyst compositions. Firstly, both formed compositions containing titanium are capable of forming TiO_2 on oxidation, either in the form anatase or rutile, or both of them. Secondly, presence of silica is expected to stabilize the fraction of anatase, in accordance with the results [43], [69]. Relatively mild post-oxidation conditions were selected, including the temperatures in the range 400-500 ^{o}C and different times. The selected XRD patterns of the oxidized samples are shown in Fig. 3.2.
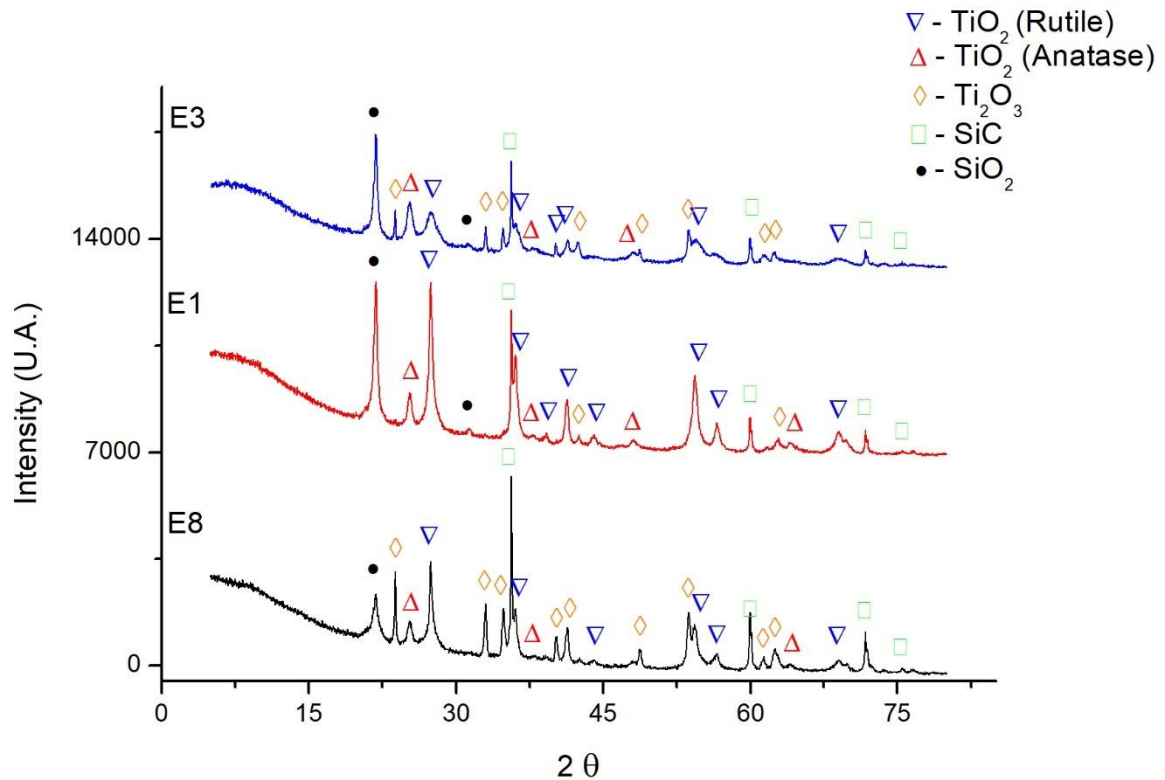
Fig. 3.2 - XRD patterns of several samples oxidized at different temperatures and for different time.

The oxidation results in vanishing of titanium oxycarbide phase and formation of both anatase and rutile polymorphs of TiO_2. Corresponding results of the XRD quantification are also shown in Table 3.2. An interesting guideline can be taken from the Fig. 3.3 where the molar quantities of anatase and rutile (Y axis), averaged for each temperature of Ar processing, are plotted against the molar concentration of titanium-containing precursors in the samples after processing in Ar. Since Ti_2O_3 and TiOC are the only Ti-containing species in Ar processed materials, it appears that the formation of both anatase and rutile is especially promoted by the presence of TiOC, while Ti_2O_3 is still present in the samples after oxidation and disappears only in extreme oxidizing conditions as 500 ^{o}C for 25 h.

Other useful guidelines for the effects of processing conditions on the phase composition of the oxidized samples can be obtained from assessing the results of Taguchi experimental planning. These results are given in Table 3.3.
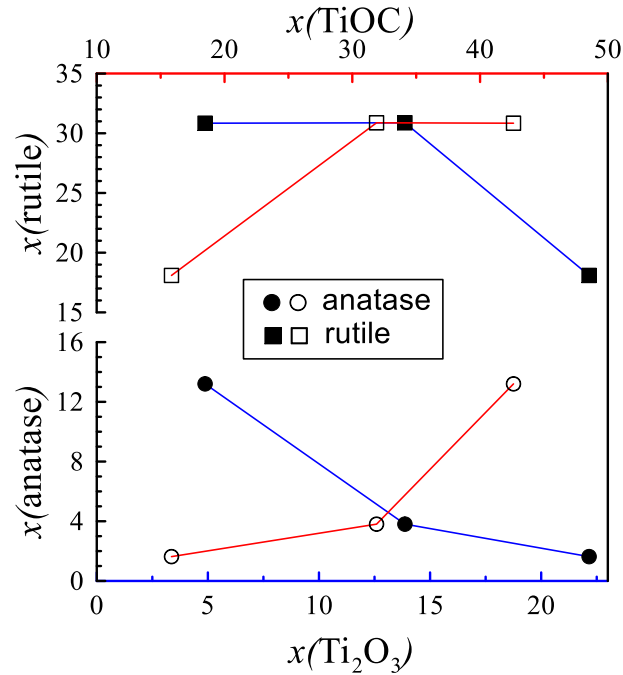
Fig. 3.3 - The effects of TiOC content (X axis) in the precursor samples after Ar treatment on the anatase and rutile content (Y axis) in the post-oxidized samples. Red and blue lines correspond to the dependencies on TiOC and Ti_2O_3 content, accordingly.

Table 3.3 - Correlation matrix for the effects of Ar-processing temperature (T_{Ar}), post-oxidation temperature (T_{ox}) and time (t_{ox}) on the molar fractions of the Ti-containing species in the oxidized samples, correlation coefficient (K_r) and corresponding coefficients (α, β, γ and Θ) of the linear regression model described by the Eq. (16).

	Correlation matrix			Kr	α (T_{Ar})	β (T_{ox})	γ (t_{ox})	Θ
	T_{Ar}	T_{ox}	t_{ox}					
$x(Ti_2O_3)$	-0.808	-0.365	-0.278	0.993	-0.146	-0.066	-0.195	230.8
x(anatase)	0.787	-0.432	-0.061	0.995	0.116	-0.064	-0.035	-115.3
x(rutile)	0.491	0.675	0.340	0.874	0.127	0.175	0.343	-221.5
$x(SiO_2)$	0.983	-0.024	-0.053	0.985	0.151	-0.004	-0.032	-167.3

The impacts of each parameter were analysed using linear regression model:

$$x(Ti_2O_3/anatase/rutile/SiO_2) = \alpha \cdot T_{Ar} + \beta \cdot T_{ox} + \gamma \cdot t_{ox} + \theta \qquad (16)$$

The correlation matrix and the values of regression coefficients obtained for the post-oxidized samples actually suggest the following trends. The processing conditions in Ar, which result in pre-reduction of titania, are extremely important for the anatase formation, namely, a higher treatment temperature facilitates the formation of anatase. Again, this correlates well with the trends in formation of titanium oxycarbide, which, for the selected post-oxidizing conditions, appears to be the main precursor for the anatase formation (Tables 3.1 and 3.2, and Fig. 3.3). The negative value for correlation factor between Ar-processing temperature and Ti_2O_3 concentration seems counterintuitive, an increase in Ti_2O_3 concentration may be expected when increasing this temperature. However, this can be explained by the fact that higher Ar processing temperature rather facilitates the formation of TiOC as compared to Ti_2O_3 (Table 3.1). Upon oxidation, TiOC is fully converted to anatase/rutile even at lowest oxidation temperature/time, while the Ti_2O_3 residuals still remain and thus suggest this type of apparent correlation. Higher oxidizing

temperature (T_{ox}) appears favourable for the rutile formation as compared to anatase, in accordance with the predictions discussed in the introduction section. The main parameter affecting the amount of SiO_2 in the post-oxidized samples is the Ar-processing temperature, as indicated by corresponding correlation factor above 0.98, while the factors for T_{ox} and t_{ox} are close to zero, indicating a very weak correlation with these parameters. The kinetics of oxidation may be illustrated by the t_{ox} parameter, showing a moderate relevance of the oxidation time for the formation of rutile and, probably, vanishing Ti_2O_3 oxide.

3.2. Microstructural evolution

Typical microstructure of the IM powder and corresponding distribution of the titania and silicon carbide particles are presented in Fig. 3.4.
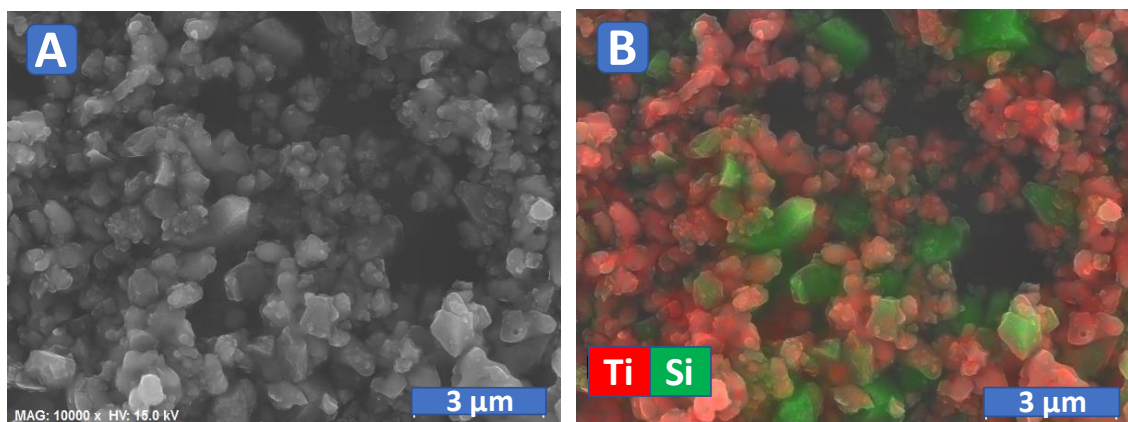
Fig. 3.4 - Microstructural characterization of the initial TiO_2 (rutile): SiC (1:1 mol.) mixture: SEM image of the powder after milling (A) and EDS mapping results for the same selected area (B).

The particles size is similar to that for initial precursor powders, where SiC is mostly of micrometric size, while TiO_2 rutile particles are of submicrometric or even nanometric (agglomerated) size. Indeed, the silicon carbide is well-known as a hard material, at it is impossible to reduce its particle size by the milling procedure employed in the present work. Still, the used milling allows for quite satisfactory homogenization, as it follows from the chemical analysis map (Fig. 3.4B).

The examples of microstructure of the ceramic samples processed under Ar atmosphere are shown in the Fig. 3.5. These results again evidence a significant porosity, which is expected to minimize oxygen diffusion limitations during following post-oxidation step. The observed microstructures suggest the presence of significant interaction between initial composite components, in agreement with the XRD results (Fig. 3.2) discussed above. In particular, one can observe the formation of core-shell-like particles with a lighter core surrounded with a darker shell, especially well-visible in the case of Fig. 3.5D. Thus, the prospective photocatalytic properties might be affected by microstructural features of the prepared materials, in addition to the phase composition.

More details regarding the composition of those core-shell particles can be revealed using EDS analysis, combined with SEM, corresponding results are presented in Fig. 3.6. This image illustrates quite typical microstructural features in the sample, processed in Ar under intermediate temperature of 1300 °C. The shell is enriched in silicon, and corresponding morphology is very similar to glassy/amorphous state. Since the silicon carbide particles have

initially absolutely different shape (Fig. 3.4B), the shell is likely composed of SiO_2, in agreement with the XRD results. Unfortunately, the used equipment and procedure do not allow to track the carbon contrast in the samples, since they required preliminary carbon deposition prior to the SEM/EDS characterization. Thus, it could be assumed that the core is composed of Ti_2O_3 and TiOC, the latter is rather likely formed closer to the surface in the space confined by the contact between initial TiO_2 and SiC particles.
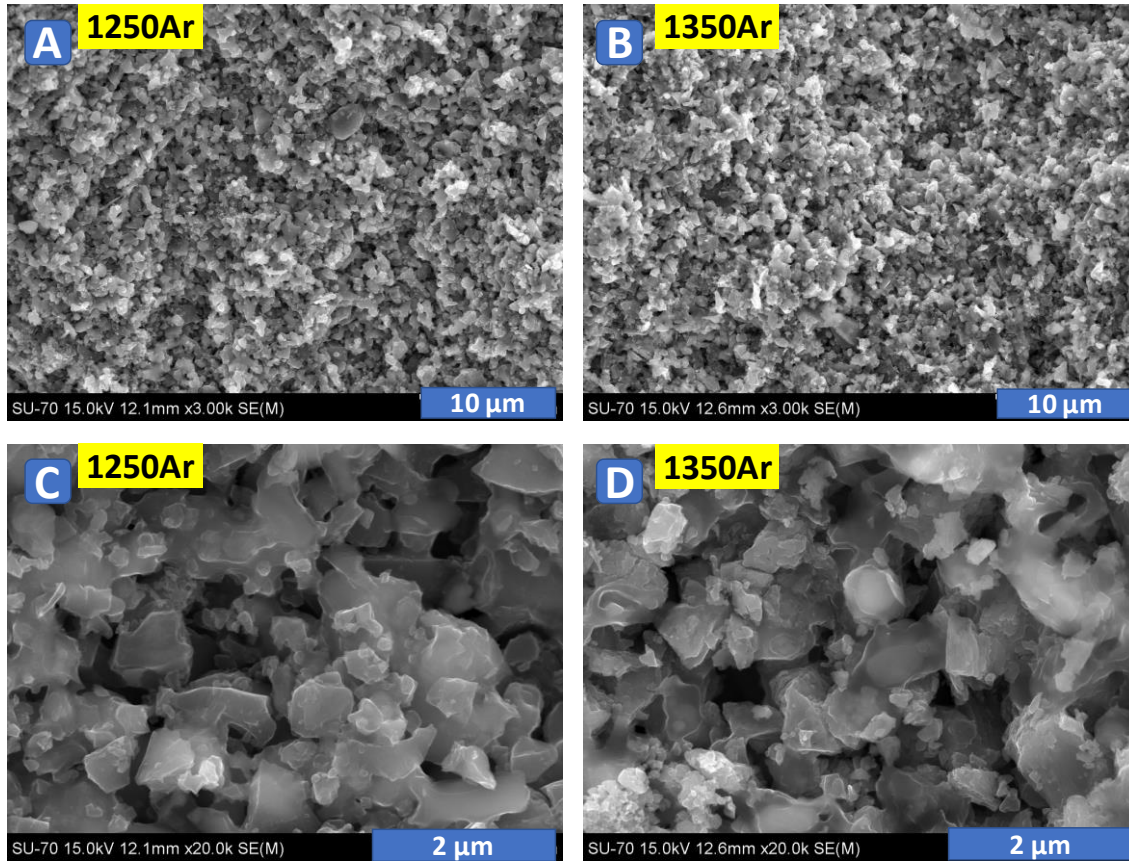
Fig. 3.5 - SEM micrographs of 1250Ar (A,C) and 1350Ar (B,D) ceramics at comparable resolution.

Some Ti-rich particle have the surface clear from SiO_2, while other particles look as completely blocked, as illustrated by the EDS maps in the Fig. 3.6.
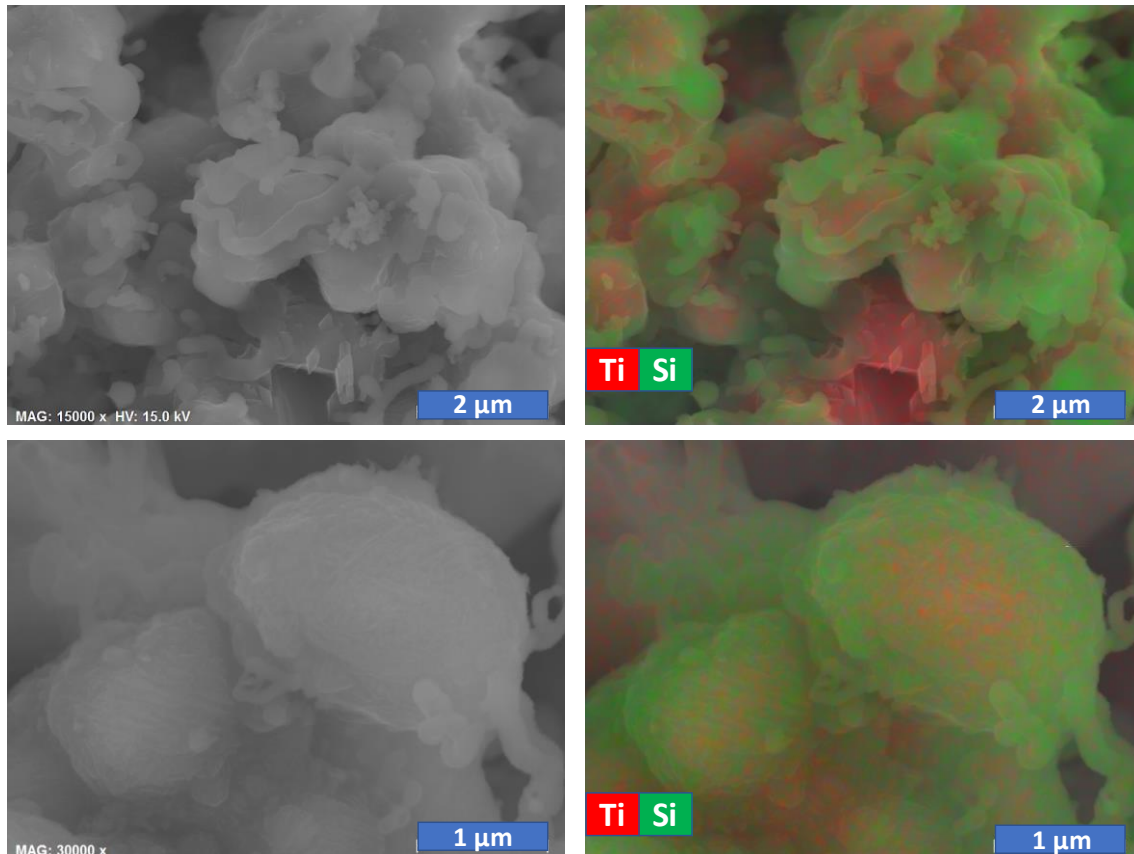
Fig. 3.6 - SEM/EDS results for the 1300Ar samples, showing the formation of core-shell structures.

Suck blocking may impede oxidation, which is necessary for the formation of anatase-containing samples from Ar-processed materials. On the other hand, it could facilitate a very delicate oxidation, which might be rather suitable for the anatase formation and nanostructuring.

The microstructural studies performed for post-oxidized samples show the formation of more open structures (Fig. 3.7A and B), while part of the Ti-rich particles still have SiO_2 surface blocking layer. Oxidation and corresponding volume increase seem at least partially to destroy the SiO_2 shell, leading to the formation of nanostructured titania polymorphs. The latter is especially well-illustrated by the results obtained for E4 oxidized sample, where columnar submicro-nanosized titania-based structures appear to grow through the silica shell.
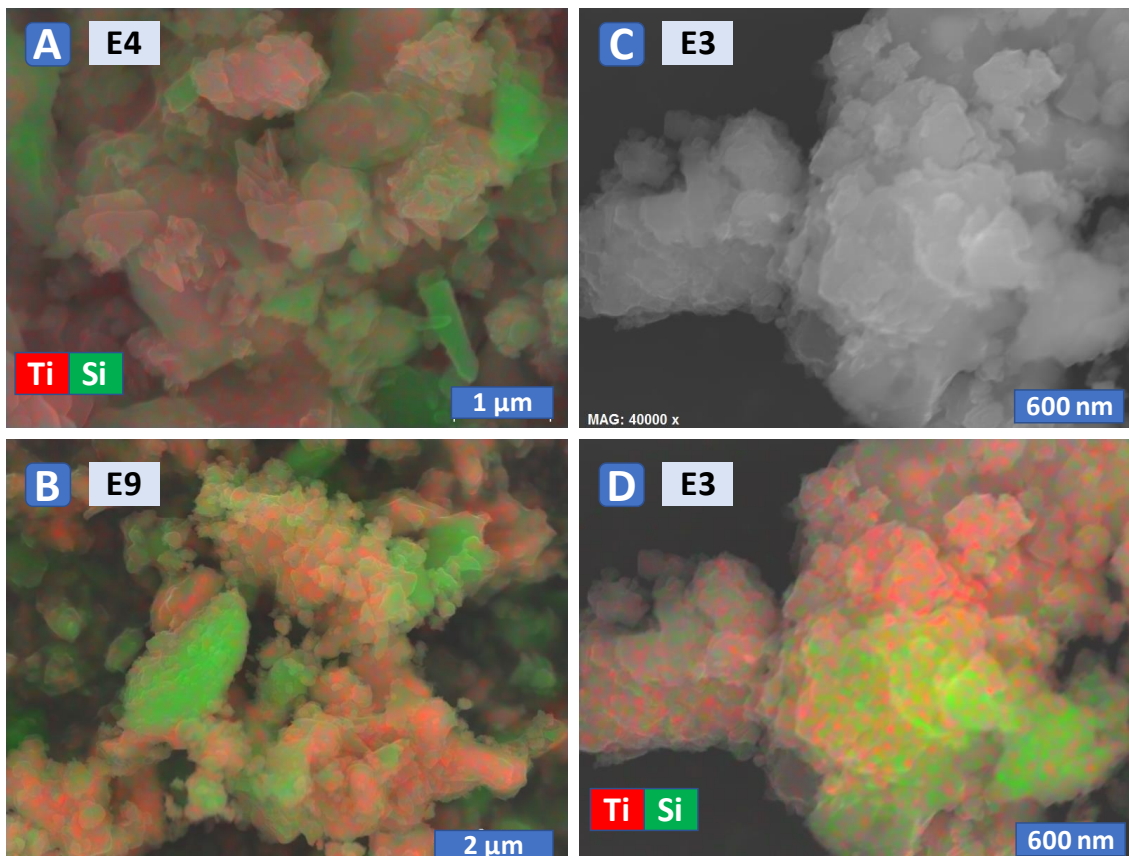
Fig. 3.7 - EDS mapping (A, B, D) and SEM (C) results for the oxidized samples: E4 (A), E9 (B), E3 (C,D).

Unfortunately, the SEM/EDS analysis does not allow to distinguish between titania polymorphs. Secondly, the observed microstructures of the oxidized samples look quite similar and do not allow to reveal any tendencies with temperature/oxidation time based only on the microstructural studies. Thus, these results basically highlight that possible promoting effects on the photocatalytic performance, imposed by the formation of anatase and rutile under oxidizing conditions, may be at least partially hindered by surface blocking layers composed of SiO_2. On the other hand, silica is known to have a promoting effect on the photocatalytic performance of titania, which involves the formation of local Ti-O-Si bonds [70]. In particular, a common strategy to benefit from this synergy includes the preparation of $SiO_2@TiO_2$ core-shell nanoparticles with enhanced activity [71]. Although the core-shell structures produced in the present work have, to a certain extent, an inversed architecture comprised of titanium-rich core and silica shell, one still can expect some synergistic effects towards photocatalysis based on TiO_2-SiO_2 interaction and formation of local Ti-O-Si linkages, invisible for XRD technique. Corresponding tests were performed and described in the next section.
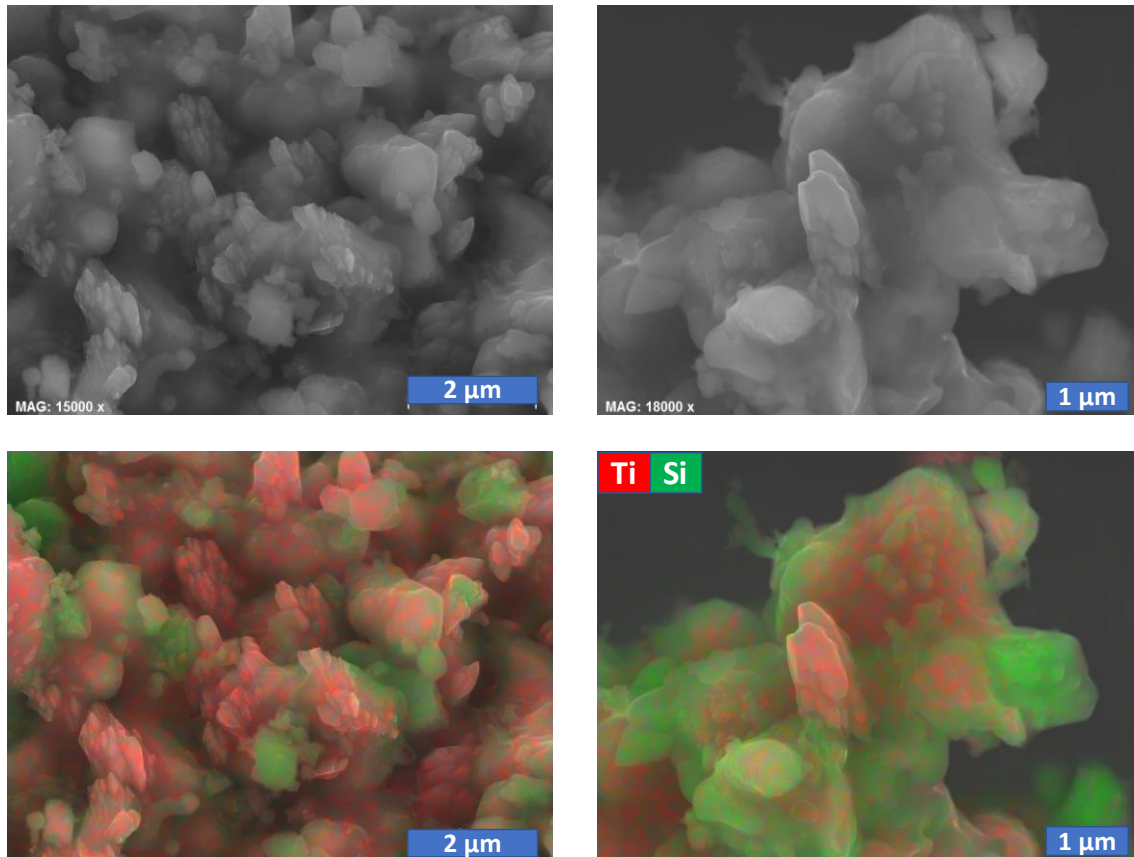
Fig. 3.8 - SEM/EDS results for E4 sample.

Further insights on the microstructural evolution can be obtained from the comparative analysis of surface area of the samples measured using BET technique. The specific surface area was calculated using BET equation (eq. 10). Below the calculation is exemplified for the sample E6. The left side of the equation (10) is plotted against the relative pressure p/p_0 (Fig. 3.9). The slope a and the intercept b are determined by linear regression. The monolayer amount is then $n_m = 1/(a+b)$. For the sample E6 the calculated value of the monolayer amount was 1.87×10^{-4} mol/g. From the equation 12 one can obtain a S_{BET} value of 18.28 m^2/g.
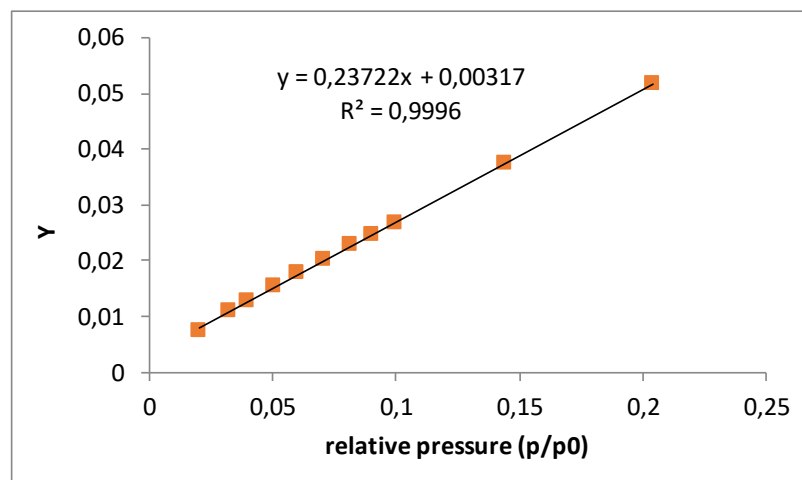
Fig. 3.9 - BET plot for sample E6 and corresponding linear fitting.

Fig. 3.10 presents the adsorption isotherms, where the amount of N_2 adsorbed/desorbed is plotted on the ordinate against the corresponding relative pressure, p/p_0, on the abscissa.

(a)

(b)

(c)

(d)

(e)
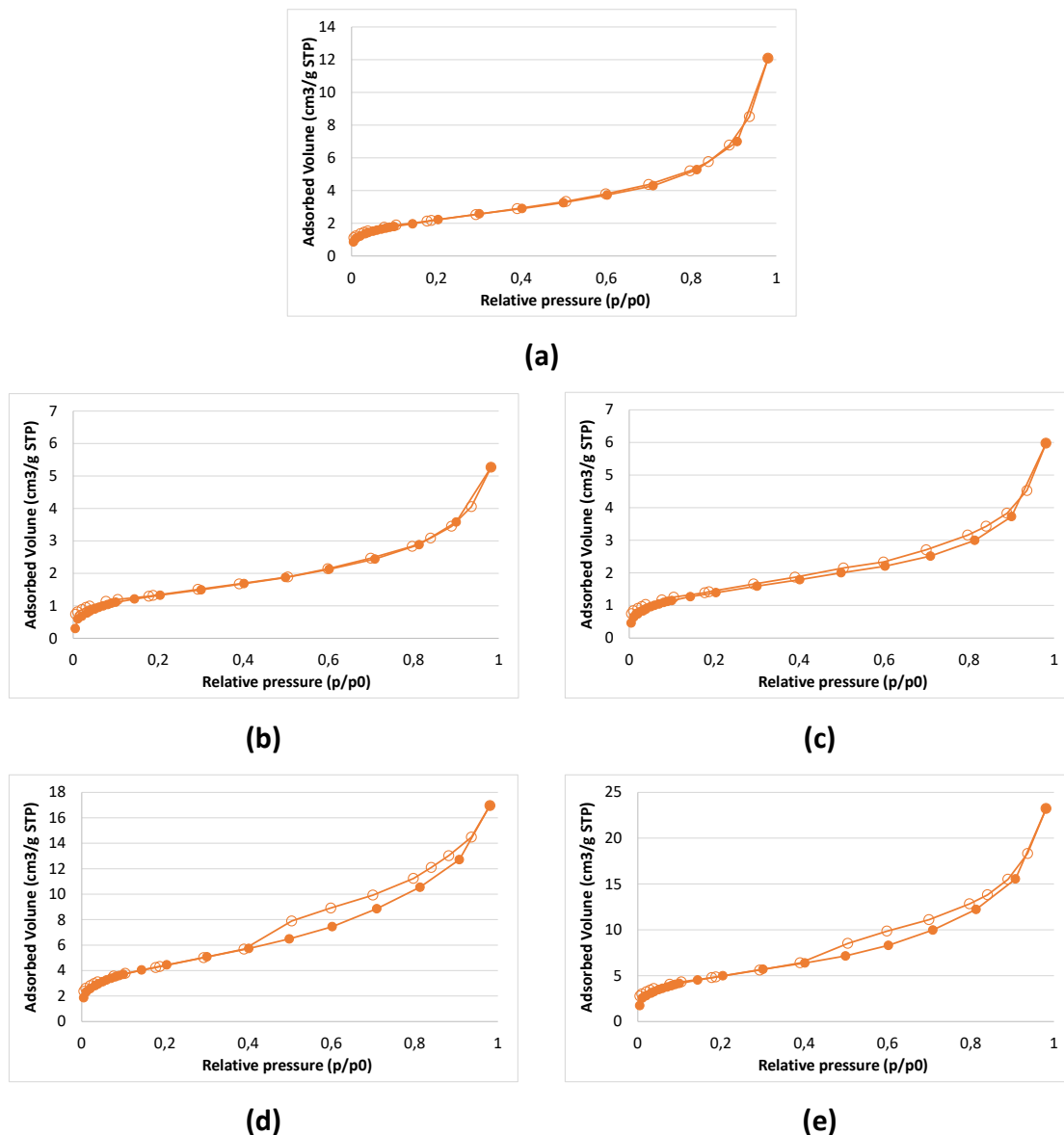
Fig. 3.10 – N_2 adsorption (full symbols) and desorption (empty symbols) isotherms for materials: (a) IM; (b) 1300red; (c) 1350red; (d) E5; (e) E6.

The N_2 adsorption-desorption isotherms of the initial mixture and reduced samples (Fig. 3.10 a-c) are type II, which is characteristic of non porous materials [72]. This is rather expected, taking into account the nature of the composite precursors powders with (sub) micrometric particle size, while the reaction between titania and silicon carbide at elevated temperature and following formation of the core-shell structures are not likely to result in appearance of the micro- and mesoporosity. On the contrary, the isotherms of oxidized samples (Fig. 3.10 d-e) present a hysteresis loop and are type IV, which is characteristic of mesoporous sorbents. The results

suggest that oxidizing conditions induce the formation of some mesoporosity (pore width in the range 2-50 nm), very likely being promoted by the growth of nanostructured anatase.

Finally, the table 3.4 presents the values of the specific surface area and total pore volume.

Table 3.4 – Specific surface area calculated using BET equation (S_{BET}) and total pore volume (V_T) calculated using Gurvitch rule.

Sample	S_{BET} (m^2/g)	V_T (cm^3/g)
E6	18.28	0.0363
E5	16.08	0.0265
1300red	4.84	0.0082
1350red	5.00	0.0093
IM	7.69	0.0189

Overall, the materials present low total porosity. The results are in excellent agreement with the SEM/EDS studies, discussed above. The formation of core-shell structures in the course of redox reaction (15) results even in a decrease of the surface area. Again, following nanostructuring in the oxidizing samples significantly enlarges the available surface, with expected impact on the photocatalytic activity.

3.3. Photocatalytic activity

For the sake of comparison, the photocatalytic studies were performed for initial IM powder, standard P25 TiO$_2$-based photocatalyst and the samples powdered after processing under Ar and air atmospheres. The Fig. 3.11 shows UV-vis spectrum of the bare fresh methylene blue solution, showing a maximum absorption peak at 664 nm. Thus, the concentration of methylene blue at a given reaction time was calculated by measuring the absorbance at 664 nm.
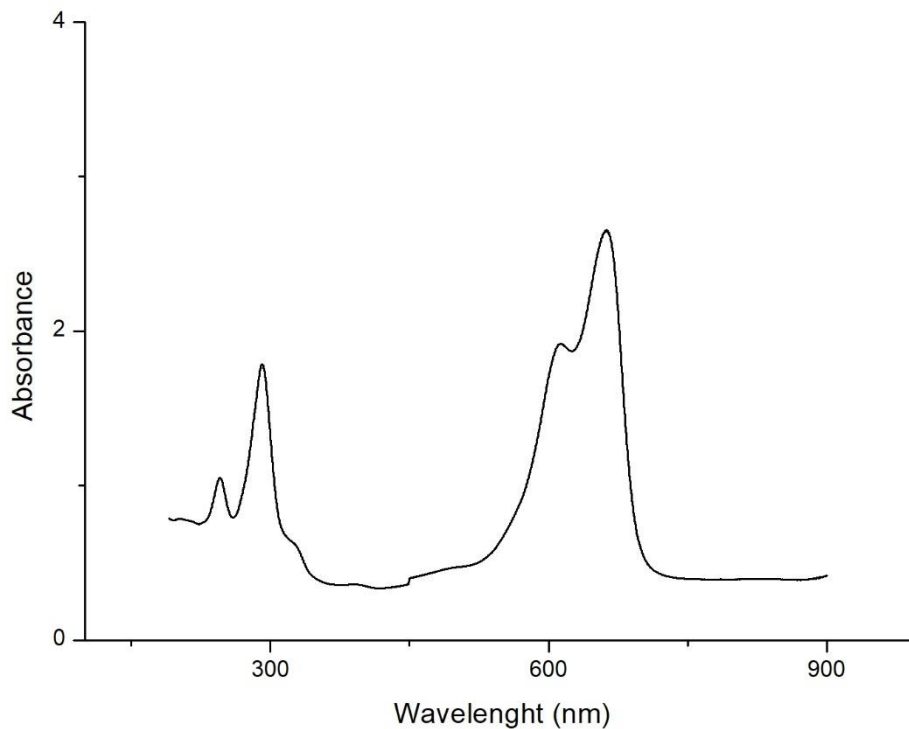
Fig. 3.11 - Uv-vis spectrum of the methylene blue solution prepared for the photocatalytic tests.

During the photocatalytic process, the photo-generated electrons and holes in the materials under study are transferred to the nearby methylene blue molecules and participate in the redox reactions resulting in the decomposition of methylene blue into H_2O and CO_2 [73], [74]. Fig. 3.12 presents a C/C_0 plot against irradiation time for several selected compositions, where C_0 is the initial concentration after dark conditions stage and C the concentration of methylene blue at different test times. The initial IM powder shows a noticeable photocatalytic activity provided by the presence of rutile; fastest photodegradation of the methylene blue was expectedly observed in the case of the standard P25 TiO_2 powder, containing anatase and rutile phases in a ratio of about 4:1. As an example, Fig. 3.13 shows typical microstructure of P25 particles, with high degree of nanostructuring and obviously higher surface area as compared to the Ar-processed and oxidized samples produced in this work (Figs. 3.5 – 3.7). The Ar-processed non-oxidized samples, containing Ti_2O_3 and TiOC, demonstrate the lowest rate of the photocatalytic degradation. Based on the results on specific surface area calculated from BET (Table 3.3), this behaviour can be attributed to the blocking of the active area, as also revealed by combined SEM/EDS studies (Figs. 3.6, 3.7). It should be noticed that, although the presence of significant amount of Ti^{3+} species may facilitate the recombination of the charge carriers and, thus, effectively suppress the photodegradation, the photoactivation process for TiOC and Ti_2O_3 phases may be actually shifted to the visible light [75]–[77], while the studies in the present work were performed using an ultraviolet lamp. This means that Ar-processed samples may still possess some photocatalytic activity under visible light, although microstructural constraints imposed by presence of silica shells are likely to counterbalance this improvement.
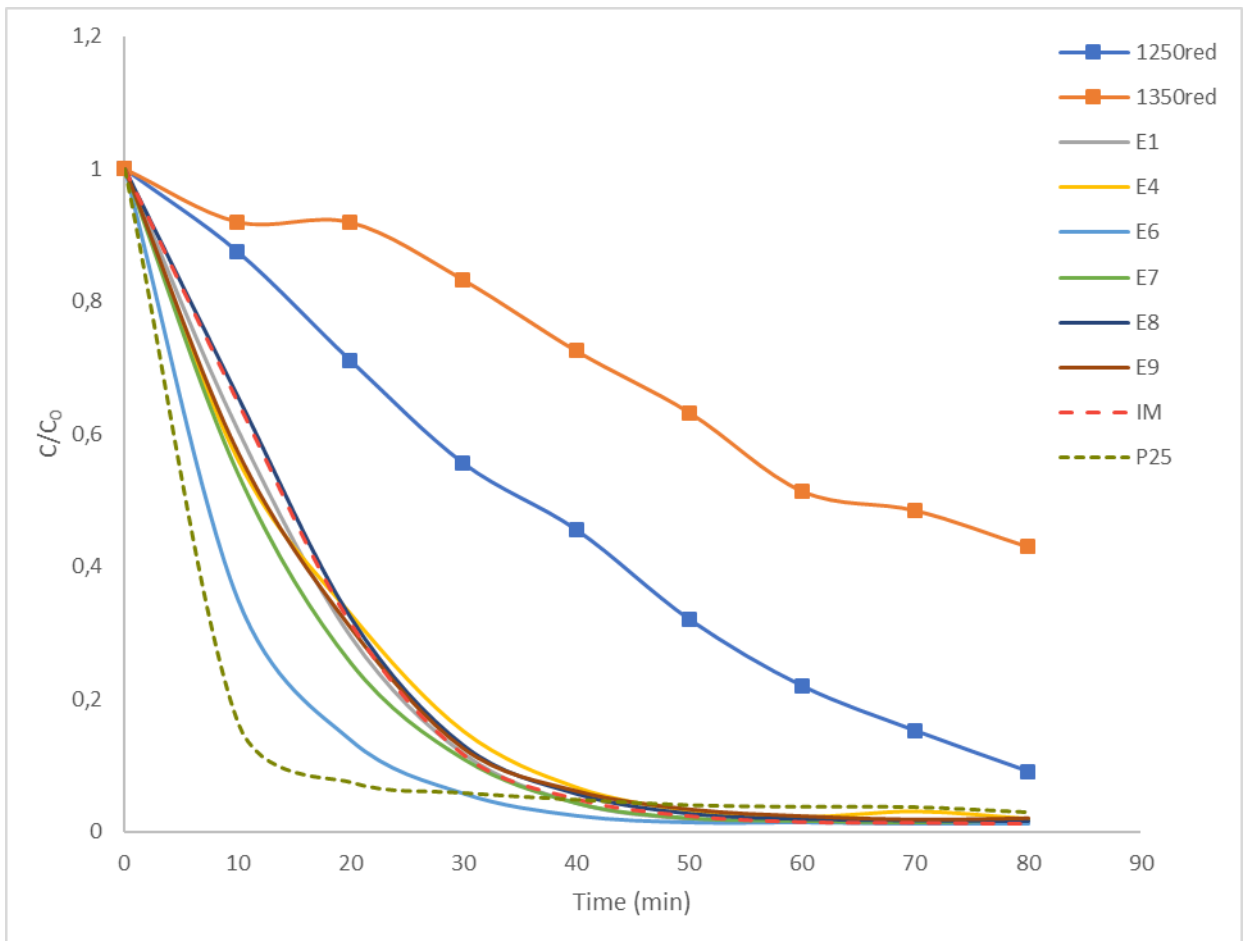
Fig. 3.12 - Methylene blue photocatalytic tests.
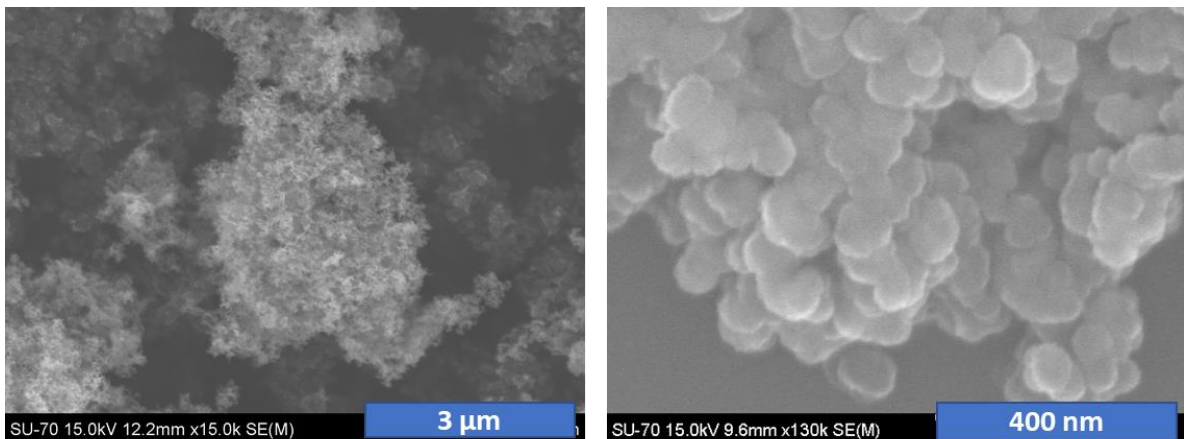
Fig. 3.13 - SEM images of the P25 powder, used as a reference in photocatalytic tests.

On the contrary, the major part of the post-oxidized samples promotes faster photodegradation of the methylene blue as compared to the initial IM mixture, in agreement with the tendencies observed for the phase composition and specific surface area. The best performance was observed for the E6 sample, prepared by processing in Ar at intermediate

temperature (1300 °C) and post-oxidized at lowest temperature (400 °C) from those selected (400-500 °C) for longest oxidation time of 25 hours. The latter may indicate that the range of processing conditions under oxidizing atmosphere should be further optimized taking into account possible kinetic limitations, if aiming on further improvement of the photocatalytic properties.

Finally, the impacts of the processing conditions on photocatalytic activity of the post-oxidized samples were analysed based on the values of apparent rate constant of the first-order kinetics (K_{ap}) and the half-life time of photocatalytic degradation ($t_{1/2}$):

$$\ln\left({C}/{C_0}\right) = K_{ap} \times t \tag{17}$$

$$t_{1/2} = \frac{\ln(2)}{K_{ap}} \tag{18}$$

The calculated values of the rate constant and half-life time are given in the Table 3.4, as well as the linear regression coefficient (R^2).

Table 3.5 - Comparison between the values of K_{ap} and the half-life time of the reference and post-oxidized and reference samples.

Photocatalytic parameters	IM	P25	E1	E2	E3	E4	E5	E6	E7	E8	E9
$K_{ap} \times 10^2$, min^{-1}	7.18	14.33	7.53	7.03	7.37	6.54	5.71	8.93	7.61	6.81	6.75
$T_{1/2}$, min	9.7	4.8	9.2	9.9	9.4	10.6	12.1	7.8	9.1	10.2	10.3
R^2	0.987	0.950	0.983	0.990	0.978	0.992	0.960	0.987	0.994	0.986	0.994

The highest K_{ap} value of 0.0893 min^{-1} and lowest $t_{1/2}$ of 7.8 min were observed for E6 sample, being ~1.6 times enhanced in terms of photocatalytic performance as compared to E5 sample and around 1.25 times compared to the initial mixture. On the other hand, in the same testing conditions, the performance of industrial P25 photocatalyst is only ~1.6 better than that for E6 sample. These results show an obvious potential for designing the performing titania-based photocatalysts using the proposed approach.

The table 3.5 presents the values of correlation factors for the effects of processing conditions on photocatalytic activity of the post-oxidized samples.

Table 3.6 - Correlation matrix for the effects of processing conditions on the photocatalytic activity of post-oxidized samples.

Parameter	T_{Ar}	T_{ox}	t_{ox}
K_{ap} (methylene blue)	0.124	-0.223	0.503
$t_{1/2}$	-0.133	0.170	-0.480

Surprisingly, but these results predict the major impact of the oxidation time on K_{ap} and $t_{1/2}$ values, while similar analysis for the phase composition (Table 3.2) suggests that the amount of Ti_2O_3, anatase, rutile and SiO_2 phases is determined by the Ar-processing and post-oxidation temperatures rather than by t_{ox}. It should be noticed that the maximum difference in the measured photocatalytic activities between E1, E2, E3, E7, E8 and IM samples corresponds to ~10%. Such a moderate variable variation may increase the errors associated with the Taguchi

plan analysis, while the relevance of the t_{ox} may be simply conditioned by the fact that the highest photocatalytic performance was observed for the sample oxidized for 25 hours. Still, besides the phase composition, the photocatalytic activity is strongly influenced by the microstructural features and availability of the surface for the reaction, which, in turn, can be affected by the formation of core-shell particles. As an example, while in several cases the formation of anatase/rutile mixture by post-oxidation is expected to be advantageous for the photodegradation reaction rate as compared to the initial mixture, partial blocking of the active surface by silica may impair this positive effect. Additional studies, described in the next section, are required to confirm the relevant mechanisms behind the observed effects of the processing conditions on the phase composition and photocatalytic performance.

4. Conclusions and future work

The prospects for designing multifunctional titania-based photocatalysts by controlled redox reactions in TiO_2-SiC mixture were assessed. The selected processing approach included a partial reduction of titania by silicon carbide in inert argon atmosphere, with an objective to produce precursors capable to form anatase in the oxidizing conditions. This was followed by a delicate oxidation under air conditions to produce TiO_2, both in the form of rutile and anatase. Taguchi experimental planning was used to evaluate the effects of processing conditions, namely, the temperature of processing in Ar (T_{Ar} – 1250, 1300 and 1350 ^{o}C), the post-oxidation temperature (T_{ox} – 400, 450, 500 ^{o}C) and time (t_{ox} – 1, 5 and 25 h) on the phase composition and photocatalytic activity. Various experimental techniques were applied to study the relevant properties of prepared composite materials, including X-Ray diffraction analysis (XRD), scanning electron microscopy (SEM) combined with energy-dispersive X-ray spectroscopy (EDS), surface area measurements by Brunauer-Emmett-Teller (BET) analysis and photocatalytic activity tests involving photodegradation of organic dye methylene blue. The main conclusions of the work are the following:

- Selected range of processing conditions in Ar and air atmospheres allowed controlled interaction between the initial composite components, leading to the formation of partially reduced titanium-containing compounds, which can be then oxidized to form rutile/anatase mixture. The final composite also retained a fraction of SiC phase, which is required for thermal co-activation functionality.

- Higher temperatures of the treatment in Ar (T_{Ar}) promoted the formation of titanium oxycarbide TiOC, which acted as a main precursor for the anatase formation in post-oxidized samples. The analysis of correlation effects in selected Taguchi experimental plan has shown that higher oxidizing temperature (T_{ox}) is more favourable for the rutile formation as compared to anatase. The effects of the treatment temperatures both in Ar and air were shown to be the most important for the phase composition, whilst the oxidation time was only moderately relevant.

- Microstructural studies have revealed the formation of core-shell microstructures in the case of the samples processed in Ar, with the shell composed of silica and the core rich in titanium-containing species. This microstructural evolution resulted in the limited surface area in these samples. Post-oxidation resulted in at least partial destruction of the SiO_2 shell, leading to the formation of nanostructured titania polymorphs and noticeable increase in the surface area.

- The phase composition and microstructural evolution in the post-oxidized samples imposed a noticeable effect on the photocatalytic performance. The activity of the best prepared material, expressed in apparent rate constant equal to 0.089 min^{-1}, was only 1.6 times lower than the corresponding activity of the nanostructured industrial P25 photocatalyst. The results of Taguchi analysis suggested oxidation time (t_{ox}) as a most impactful parameter of the selected processing conditions on the photocatalytic activity.

Future work on this approach for designing composite TiO_2-based photocatalysts may include:
- Photocatalytic tests for the same materials using different organic dye, to avoid any specific effects related to the methylene blue. Corresponding work is ongoing for Rhodamine B. The

objective is to understand better the factors affecting the photocatalytic performance, because the Taguchi analysis of the effects of processing conditions on the phase composition suggest the Ar-treatment and oxidation temperature as the most relevant parameters, while oxidation time appears more relevant for photocatalytic activity. This discrepancy should be further addressed.

- Selection of a wider range of oxidation temperature / time for Taguchi experimental design, to cover the conditions where the titanium-containing phases are shifted either to anatase, or rutile polymorph. This is expected to produce a larger difference in the photocatalytic activity of the post-oxidized samples, thus allowing a better quantification of the relevant effects.
- Selection of a different (particle size, morphology) SiC/TiO_2 precursors to try to avoid the formation of core-shell structures, blocking the active surface.
- Tests of the optimized materials for NO_x abatement.

Bibliography

[1]   A. Ibhadon and P. Fitzpatrick, "Heterogeneous Photocatalysis: Recent Advances and Applications," *Catalysts*, vol. 3, no. 1, pp. 189–218, 2013.

[2]   S. Banerjee, S. C. Pillai, P. Falaras, K. E. O'shea, J. A. Byrne, and D. D. Dionysiou, "New insights into the mechanism of visible light photocatalysis," *J. Phys. Chem. Lett.*, vol. 5, no. 15, pp. 2543–2554, 2014.

[3]   A. Kudo and Y. Miseki, "Heterogeneous photocatalyst materials for water splitting," *Chem. Soc. Rev.*, vol. 38, no. 1, pp. 253–278, 2009.

[4]   J. Ângelo, L. Andrade, L. M. Madeira, and A. Mendes, "An overview of photocatalysis phenomena applied to NOxabatement," *J. Environ. Manage.*, vol. 129, no. x, pp. 522–539, 2013.

[5]   K. Hashimoto, H. Irie, and A. Fujishima, "TiO 2 Photocatalysis: A Historical Overview and Future Prospects," *Jpn. J. Appl. Phys.*, vol. 44, no. 12, pp. 8269–8285, 2005.

[6]   M. Pelaez *et al.*, "A review on the visible light active titanium dioxide photocatalysts for environmental applications," *Appl. Catal. B Environ.*, vol. 125, pp. 331–349, 2012.

[7]   N. Yahya *et al.*, "A review of integrated photocatalyst adsorbents for wastewater treatment," *J. Environ. Chem. Eng.*, vol. 6, no. 6, pp. 7411–7425, 2018.

[8]   O. Frank E., "Inorganic materials as catalysts for photochemical splitting of water," *Chem. Mater.*, vol. 20, no. 1, pp. 35–54, 2007.

[9]   L. Wang, J. Zhao, H. Liu, and J. Huang, "Design, modification and application of semiconductor photocatalysts," *J. Taiwan Inst. Chem. Eng.*, vol. 93, pp. 590–602, 2018.

[10]   D. A. H. Hanaor and C. C. Sorrell, "Review of the anatase to rutile phase transformation," *J. Mater. Sci.*, vol. 46, no. 4, pp. 855–874, 2011.

[11]   C. Byrne, G. Subramanian, and S. C. Pillai, "Recent advances in photocatalysis for environmental applications," *J. Environ. Chem. Eng.*, no. July, pp. 0–1, 2017.

[12]   R. Fagan, D. E. McCormack, D. D. Dionysiou, and S. C. Pillai, "A review of solar and visible light active TiO2photocatalysis for treating bacteria, cyanotoxins and contaminants of emerging concern," *Mater. Sci. Semicond. Process.*, vol. 42, pp. 2–14, 2016.

[13]   B. Eggins, "Photocatalytic treatment of humic substances in drinking water," *Water Res.*, vol. 31, no. 5, pp. 1223–1226, 1997.

[14]   J. E. S. Haggerty *et al.*, "High-fraction brookite films from amorphous precursors," *Sci. Rep.*, vol. 7, no. 1, pp. 1–11, 2017.

[15]   T. Ohno, K. Sarukawa, and M. Matsumura, "Photocatalytic Activities of Pure Rutile Particles Isolated from TiO 2 Powder by Dissolving the Anatase Component in HF Solution," *J. Phys. Chem. B*, vol. 105, no. 12, pp. 2417–2420, 2001.

[16]   M. Xing, W. Fang, M. Nasir, Y. Ma, J. Zhang, and M. Anpo, "Self-doped Ti3+-enhanced TiO2 nanoparticles with a high-performance photocatalysis," *J. Catal.*, vol. 297, pp. 236–243, 2013.

[17]   C. Tang, D. Zhou, and Q. Zhang, "Synthesis and characterization of Magneli phases: Reduction of TiO2in a decomposed NH3atmosphere," *Mater. Lett.*, vol. 79, pp. 42–44, 2012.

[18]   Y. Fan *et al.*, "Preparation of monophasic titanium sub-oxides of Magnéli phase with enhanced thermoelectric performance," *J. Eur. Ceram. Soc.*, vol. 38, no. 2, pp. 507–513, 2018.

[19]   X. Mao, F. Yuan, A. Zhou, and W. Jing, "Magnéli phases TinO2n−1as novel ozonation catalysts for effective mineralization of phenol," *Chinese J. Chem. Eng.*, vol. 26, no. 9, pp. 1978–1984, 2018.

[20]   A. Beltrán, L. Gracia, and J. Andrés, "Density functional theory study of the brookite surfaces and phase transitions between natural titania polymorphs," *J. Phys. Chem. B*, vol.

110, no. 46, pp. 23417–23423, 2006.

[21] H. Zhang and J. F. Banfield, "Thermodynamic analysis of phase stability of nanocrystalline titania," *J. Mater. Chem.*, vol. 8, no. 9, pp. 2073–2076, 1998.

[22] A. Sclafani and J. M. Herrmann, "Comparison of the photoelectronic and photocatalytic activities of various anatase and rutile forms of titania in pure liquid organic phases and in aqueous solutions," *J. Phys. Chem.*, vol. 100, no. 32, pp. 13655–13661, 1996.

[23] J. Augustynski, "The role of the surface intermediates in the photoelectrochemical behaviour of anatase and rutile TiO2," *Electrochim. Acta*, vol. 38, no. 1, pp. 43–46, 1993.

[24] J. Sun, L. Gao, and Q. Zhang, "Synthesizing and Comparing the Photocatalytic Properties of High Surface Area Rutile and Anatase Titania Nanoparticles," *J. Am. Ceram. Soc.*, vol. 86, no. 10, pp. 1677–1682, 2003.

[25] T. Ohno, D. Haga, K. Fujihara, K. Kaizaki, and M. Matsumura, "Unique Effects of Iron(III) Ions on Photocatalytic and Photoelectrochemical Properties of Titanium Dioxide," *J. Phys. Chem. B*, vol. 101, no. 33, pp. 6415–6419, 1997.

[26] R. R. Bacsa and J. Kiwi, "Effect of rutile phase on the photocatalytic properties of nanocrystalline titania during the degradation of p-coumaric acid," *Appl. Catal. B Environ.*, vol. 16, no. 1, pp. 19–29, 1998.

[27] Q. Wang, Z. Qiao, P. Jiang, J. Kuang, W. Liu, and W. Cao, "Hydrothermal synthesis and enhanced photocatalytic activity of mixed-phase TiO 2 powders with controllable anatase/rutile ratio," *Solid State Sci.*, 2018.

[28] J. Li, X. Xu, X. Liu, W. Qin, M. Wang, and L. Pan, "Metal-organic frameworks derived cake-like anatase/rutile mixed phase TiO2for highly efficient photocatalysis," *J. Alloys Compd.*, vol. 690, pp. 640–646, 2017.

[29] H. Zhang and J. F. Banfield, "Size Dependence of the Kinetic Rate Constant for Phase Transformation in TiO 2 Nanoparticles," *Chem. Mater.*, vol. 17, no. 13, pp. 3421–3425, 2005.

[30] A. NAVROTSKY and O. J. KLEPPA, "Enthalpy of the Anatase-Rutile Transformation," *J. Am. Ceram. Soc.*, vol. 50, no. 11, pp. 626–626, 1967.

[31] C. N. R. Rao, "Kinetics and thermodynamics of the crystal structure transformations of spectroscopically pure anatase to rutile," *Can. J. Chem*, vol. 39, pp. 498–500, 1961.

[32] S.-C. Liao, J. Colaizzi, Y. Chen, B. H. Kear, and W. E. Mayo, "Refinement of Nanoscale Grain Structure in Bulk Titania via a Transformation-Assisted Consolidation (TAC) Method," *J. Am. Ceram. Soc.*, vol. 83, no. 9, pp. 2163–2169, 2000.

[33] D. Meng *et al.*, "High Pressure Response of Rutile Polymorphs and Its Significance for Indicating the Subduction Depth of Continental Crust," *Acta Geol. Sin. - English Ed.*, vol. 82, no. 2, pp. 371–376, 2008.

[34] S. Riyas, G. Krishnan, and P. N. M. Das, "Anatase–rutile transformation in doped titania under argon and hydrogen atmospheres," *Adv. Appl. Ceram.*, vol. 106, no. 5, pp. 255–264, 2007.

[35] D. G. Syarif, A. Miyashita, T. Yamaki, T. Sumita, Y. Choi, and H. Itoh, "Preparation of anatase and rutile thin films by controlling oxygen partial pressure," *Appl. Surf. Sci.*, vol. 193, no. 1–4, pp. 287–292, 2002.

[36] N. Serpone, "Is the band gap of pristine TiO2 narrowed by anion- and cation-doping of titanium dioxide in second-generation photocatalysts?," *J. Phys. Chem. B*, vol. 110, no. 48, pp. 24287–24293, 2006.

[37] K. T. Ranjit, H. Cohen, I. Willner, S. Bossmann, and A. M. Braun, "Lanthanide oxide-doped titanium dioxide: effective photocatalysts for the degradation of organic pollutants," *J. Mater. Sci.*, vol. 34, no. 21, pp. 5273–5280, 1999.

[38] B. Sun, A. V. Vorontsov, and P. G. Smirniotis, "Role of platinum deposited on TiO2 in phenol photocatalytic oxidation," *Langmuir*, vol. 19, no. 8, pp. 3151–3156, 2003.

[39]   M. I. Franch, J. Peral, X. Domènech, and J. A. Ayllón, "Aluminium(<scp>iii</scp>) adsorption: a soft and simple method to prevent TiO $_2$ deactivation during salicylic acid photodegradation," *Chem. Commun.*, no. 14, pp. 1851–1853, 2005.

[40]   K. Okada, N. Yamamoto, Y. Kameshima, A. Yasumori, and K. J. D. MacKenzie, "Effect of Silica Additive on the Anatase-to-Rutile Phase Transition," *J. Am. Ceram. Soc.*, vol. 84, no. 7, pp. 1591–1596, 2004.

[41]   J. Yang and J. M. . Ferreira, "Inhibitory effect of the Al2O3–SiO2 mixed additives on the anatase–rutile phase transformation," *Mater. Lett.*, vol. 36, no. 5–6, pp. 320–324, 1998.

[42]   J. Yang, Y. X. Huang, and J. M. F. Ferreira, "Inhibitory effect of alumina additive on the titania phase transformation of a sol-gel-derived powder," *J. Mater. Sci. Lett.*, vol. 16, no. 23, pp. 1933–1935, 1997.

[43]   D. M. Tobaldi, A. Tucci, A. S. Škapin, and L. Esposito, "Effects of SiO2addition on TiO2crystal structure and photocatalytic activity," *J. Eur. Ceram. Soc.*, vol. 30, no. 12, pp. 2481–2490, 2010.

[44]   X. Zhang *et al.*, "Photocatalytic and photoelectrochemical studies on N-doped TiO2photocatalyst," *J. Photochem. Photobiol. A Chem.*, vol. 202, no. 1, pp. 39–47, 2009.

[45]   D. M. Tobaldi, A. Sever Škapin, R. C. Pullar, M. P. Seabra, and J. A. Labrincha, "Titanium dioxide modified with transition metals and rare earth elements: Phase composition, optical properties, and photocatalytic activity," *Ceram. Int.*, vol. 39, no. 3, pp. 2619–2629, 2013.

[46]   D. M. Tobaldi, R. C. Pullar, A. S. Škapin, M. P. Seabra, and J. A. Labrincha, "Visible light activated photocatalytic behaviour of rare earth modified commercial TiO2," *Mater. Res. Bull.*, vol. 50, pp. 183–190, 2014.

[47]   H. Wang and J. P. Lewis, "Second-generation photocatalytic materials: Anion-doped TiO2," *J. Phys. Condens. Matter*, vol. 18, no. 2, pp. 421–434, 2006.

[48]   T. Bak, J. Nowotny, M. Rekas, and C. C. Sorrell, "Defect chemistry and semiconducting properties of titanium dioxide: I. Intrinsic electronic equilibrium," *J. Phys. Chem. Solids*, vol. 64, no. 7, pp. 1043–1056, 2003.

[49]   T. Bak, J. Nowotny, M. Rekas, and C. C. Sorrell, "Defect chemistry and semiconducting properties of titanium dioxide: II. Defect diagrams," *J. Phys. Chem. Solids*, vol. 64, no. 7, pp. 1057–1067, 2003.

[50]   T. Bak, J. Nowotny, M. Rekas, and C. C. Sorrell, "Defect chemistry and semiconducting properties of titanium dioxide: III. Mobility of electronic charge carriers," *J. Phys. Chem. Solids*, vol. 64, no. 7, pp. 1069–1087, 2003.

[51]   "Kinetics of the anatase rutile transformation." .

[52]   Y. IIDA and S. OZAKI, "Grain Growth and Phase Transformation of Titanium Oxide During Calcination," *J. Am. Ceram. Soc.*, vol. 44, no. 3, pp. 120–127, 1961.

[53]   - Knoll, "Compilation of Literature Data on the Effect of Impurities on Transformation of Anatase Investigator Additive DTA Tt, ("C)," no. August, 1965.

[54]   R. Plugaru, A. Cremades, and J. Piqueras, "The effect of annealing in different atmospheres on the lumienscence of polycrystalline TiO2," *J. Phys. Condens. Matter*, vol. 16, no. 2, 2004.

[55]   A. C. Mitra, M. Jawarkar, T. Soni, and G. R. Kiranchand, "Implementation of Taguchi Method for Robust Suspension Design," *Procedia Eng.*, vol. 144, pp. 77–84, 2016.

[56]   R. Pundir, G. H. V. C. Chary, and M. G. Dastidar, "Application of Taguchi method for optimizing the process parameters for the removal of copper and nickel by growing Aspergillus sp.," *Water Resour. Ind.*, vol. 20, pp. 83–92, 2018.

[57]   V. S. Jatti, "Multi-characteristics optimization in EDM of NiTi alloy, NiCu alloy and BeCu alloy using Taguchi's approach and utility concept," *Alexandria Eng. J.*, vol. 57, no. 4, pp. 2807–2817, 2018.

[58]   M. B. Silva, C. A. Baldan, J. L. Rosa, M. P. Peres, and A. Robin, "Electrodeposition of copper

on titanium wires: Taguchi experimental design approach," *J. Mater. Process. Technol.*, vol. 209, no. 3, pp. 1181–1188, 2008.

[59] A. R. Khoei, I. Masters, and D. T. Gethin, "Design optimisation of aluminium recycling processes using Taguchi technique," *J. Mater. Process. Technol.*, vol. 127, no. 1, pp. 96–106, 2002.

[60] M. F. Sanches, N. Vitorino, J. C. C. Abrantes, J. R. Frade, J. B. Rodrigues Neto, and D. Hotza, "Effects of processing parameters on cellular ceramics obtained by paraffin emulsified suspensions," *Ceram. Int.*, vol. 40, no. 7 PART A, pp. 9045–9053, 2014.

[61] B. A. E. Ben-Arfa, I. M. Miranda Salvado, J. R. Frade, and R. C. Pullar, "Guidelines to adjust particle size distributions by wet comminution of a bioactive glass determined by Taguchi and multivariate analysis," *Ceram. Int.*, vol. 45, no. 3, pp. 3857–3863, 2018.

[62] W. H. Yang and Y. S. Tarng, "Design optimization of cutting parameters for turning operations based on the Taguchi method," *J. Mater. Process. Technol.*, vol. 84, no. 1–3, pp. 122–129, 1998.

[63] J. T. Tsai, J. C. Fang, and J. H. Chou, "Optimized task scheduling and resource allocation on cloud computing environment using improved differential evolution algorithm," *Comput. Oper. Res.*, vol. 40, no. 12, pp. 3045–3055, 2013.

[64] I. Standard, "International Standard Iso," vol. 2004, 2004.

[65] S. J. Gregg and K. S. W. Sing, "Gregg_1982_adsorption_surface_area_and_porosity.pdf." 1982.

[66] B. Mazinani, A. K. Masrom, A. Beitollahi, and R. Luque, "Photocatalytic activity, surface area and phase modification of mesoporous SiO2-TiO2 prepared by a one-step hydrothermal procedure," *Ceram. Int.*, vol. 40, no. 8 PART A, pp. 11525–11532, 2014.

[67] A. Maitre, D. Tetard, and P. Lefort, "Role of some technological parameters during carburizing titanium dioxide," *J. Eur. Ceram. Soc.*, vol. 20, no. 1, pp. 15–22, 2002.

[68] L. M. Berger, E. Langholf, K. Jaenicke-Rößler, and G. Leitner, "Mass spectrometric investigations on the carbothermal reduction of titanium dioxide," *J. Mater. Sci. Lett.*, vol. 18, no. 17, pp. 1409–1412, 1999.

[69] J. Feltrin, A. De Noni, D. Hotza, and J. R. Frade, "Design guidelines for titania-silica-alumina ceramics with tuned anatase to rutile transformation," *Ceram. Int.*, vol. 45, no. 5, pp. 5179–5188, 2019.

[70] X. Gao and I. E. Wachs, "Titania-silica as catalysts: Molecular structural characteristics and physico-chemical properties," *Catal. Today*, vol. 51, no. 2, pp. 233–254, 1999.

[71] C. C. J. Alcântara *et al.*, "Enhanced photocatalytic properties of core@shell SiO 2 @TiO 2 nanoparticles," *Appl. Catal. B Environ.*, vol. 179, pp. 333–343, 2015.

[72] M. Thommes *et al.*, "Physisorption of gases, with special reference to the evaluation of surface area and pore size distribution (IUPAC Technical Report)," *Pure Appl. Chem.*, vol. 87, no. 9–10, pp. 1051–1069, 2015.

[73] H. Atout *et al.*, "Enhanced photocatalytic degradation of methylene blue: Preparation of TiO2/reduced graphene oxide nanocomposites by direct sol-gel and hydrothermal methods," *Mater. Res. Bull.*, vol. 95, no. August, pp. 578–587, 2017.

[74] A. Houas, H. Lachheb, M. Ksibi, E. Elaloui, C. Guillard, and J. M. Herrmann, "Photocatalytic degradation pathway of methylene blue in water," *Appl. Catal. B Environ.*, vol. 31, no. 2, pp. 145–157, 2001.

[75] H. Liu, W. Yang, Y. Ma, and J. Yao, "Extended visible light response of binary TiO2-Ti 2O3 photocatalyst prepared by a photo-assisted sol-gel method," *Appl. Catal. A Gen.*, vol. 299, no. 1–2, pp. 218–223, 2006.

[76] Y. Liu, J. Wang, P. Yang, and K. Matras-Postolek, " Self-modification of TiO 2 one-dimensional nano-materials by Ti 3+ and oxygen vacancy using Ti 2 O 3 as precursor ," *RSC Adv.*, vol. 5, no. 76, pp. 61657–61663, 2015.

[77]   S. Guan, L. Hao, H. Yoshida, F. Pan, H. Asanuma, and Y. Lu, "Enhanced photocatalytic activity of photocatalyst coatings by heat treatment in carbon atmosphere," *Mater. Lett.*, vol. 167, pp. 43–46, 2016.